arXiv:astro-ph/0303325v1 14 Mar 2003

New optical and near-infrared Surface Brightness Fluctuations models. A primary distance indicator ranging from Globular Clusters to distant galaxies?

Cantiello M.[1,2], Raimondo G.[1,3], Brocato E.[1,4], Capaccioli M.[5,6]

ABSTRACT

We present new theoretical models for Surface Brightness Fluctuations (SBF) both for optical and near-infrared bands in standard ground-based and Hubble Space Telescope filter systems. Simple Stellar Population simulations are adopted. Models cover the age and metallicity ranges from $t = 5$ to 15 Gyr and from $Z = 0.0001$ to 0.04 respectively. Effects due to the variation of the Initial Mass Function and the stellar color-temperature relations are explored. Particular attention is devoted to very bright stars in the color-magnitude diagram and to investigate the effects of mass loss along the Red Giant Branch (RGB) and the Asymptotic Giant Branch (AGB). It is found that U and B bands SBF amplitudes are powerful diagnostics for the morphology of the Horizontal Branch and the Post-AGB stars population. We point out that a careful treatment of mass loss process along the RGB and AGB is fundamental in determining reliable SBF evaluations.

The SBF measurements are used to give robust constraints on the evolution of AGB stars, suggesting that mass loss activity on AGB stars should be twice more efficient than on the RGB stars.

Our models are able to reproduce the absolute SBF magnitudes of the Galactic Globular Clusters and of galaxies, and their integrated colors. New calibrations of absolute SBF magnitude in V, R, I, and K photometric filters are provided, which appear reliable enough to directly gauge distances bypassing other distance indicators.

The SBF technique is also used as stellar population tracer to derive age and metallicity of a selected sample of galaxies of known distances. Finally, *SBF color* versus *integrated color* diagrams are proposed as particularly useful in removing the well known *age-metallicity degeneracy* affecting our knowledge of remote stellar systems.

[1]INAF–Osservatorio Astronomico di Collurania, Via M. Maggini, I-64100 Teramo, Italy

[2]Dipartimento di Fisica "E.R. Caianiello", Università di Salerno and INFN, Sezione di Napoli, Gruppo Collegato di Salerno, Via S. Allende, 84081 Baronissi, Salerno, Italy; cantiello@te.astro.it

[3]Dipartimento di Fisica, Università La Sapienza, P.le Aldo Moro 2, I-00185 Roma, Italy; raimondo@te.astro.it

[4]Istituto Nazionale di Fisica Nucleare, LNGS, L'Aquila, Italy; brocato@te.astro.it

[5]Dipartimento di Scienze Fisiche, Università di Napoli Federico II, Complesso Monte S. Angelo, via Cintia, I-80126, Napoli, Italy; capaccioli@na.astro.it

[6]INAF–Osservatorio Astronomico di Capodimonte, via Moiariello 16, I-80131 Napoli, Italy

Subject headings: distance scale — globular clusters: general — galaxies: stellar content — galaxies: distances and redshifts

1. Introduction

Our understanding of external galaxies, which are milestones in the cosmological evolution, relies on the ability of gauging their distances, ages, and chemical compositions. Surface Brightness Fluctuations (SBF) are recognized as a powerful tool for providing accurate answers to all these challenges (Tonry, Ajhar & Luppino 1990: TAL90; Buzzoni 1993: B93; Worthey 1993: W93; Brocato, Capaccioli & Condelli 1998; Blakeslee, Ajhar & Tonry 1999; Liu, Charlot & Graham 2000: LCG00; Blakeslee, Vazdekis & Ajhar 2001: BVA01). Since the first attempt of using the SBF in galaxies to estimate cosmic distances (Tonry & Schneider 1988: TS88), a major observational effort has been made to improve the accuracy of the method (TAL90; Luppino & Tonry 1993; Lorenz et al. 1993; Tonry et al. 1997: TBAD97). As a matter of fact, the typical uncertainties on the distances derived via the SBF are of the order of 10% or less (Mei, Quinn & Silva 2001). Moreover, SBF work well in a wide range of distances, from the Local Group objects out to galaxy clusters such as Virgo, Fornax, and even Coma. Recently Jensen et al. (2001) succeeded in reaching galaxies at 150 Mpc ($H_0 = 75\ km\ s^{-1} Mpc^{-1}$) using near-infrared (NIR) HST data.

The largest SBF database available so far is that of Tonry & collaborators (Tonry et al. 2001: T01, and references therein). They measured the I-band SBF of nearly 300 galaxies, and were able to calibrate empirically the absolute SBF amplitude in this same band with reference to Cepheids-derived distances. The calibrations in other bands have been provided: by BVA01 in V-band in the K-band by Liu, Graham & Charlot (2002: LGC02), and in the $F160W$-band by Jensen et al. (2003). Relying upon measurements of dwarf elliptical galaxies (e.g. Jerjen, Freeman & Binggeli 1998; Jerjen, Binggeli & Freeman 2000), Jerjen et al. (2001) calibrated the R-band SBF absolute magnutide versus the galaxy $(B-R)_0$ color.

This paper provides a new approach to derive SBF for Simple Stellar Populations (SSPs, see Renzini & Buzzoni 1986). Our first goal is to revise the theoretical calibrations of absolute magnitudes of the optical and NIR SBF. The reason is that empirical calibrations rest on some other indicators, thus confining SBF to the role of at least secondary distance indicators (SBF errors sum up to the uncertainties of the primary distance indicators). Such a limitation may be removed by theoretical SBF models which, by providing *absolute galaxy SBF magnitude* versus *integrated color* relations for several different filters, set the SBF method into the class of *primary distance indicators*. Of course one needs a high degree of reliability for the adopted theoretical framework.

A second goal is to probe the capability of our SBF models in analyzing the stellar content

of star clusters and galaxies as a complementary tool to the *classical* method based on integrated magnitudes and colors. Unfortunately, disentangling the information on the main physical quantities which define the dominant stellar populations, the formation, and the evolution processes in elliptical and spiral galaxies from their integrated broad-band colors and spectral features still remains an intriguing problem (Brocato et al. 1990; Weiss, Peletier & Matteucci 1995; Bressan, Chiosi & Tantalo 1996; Kobayashi & Arimoto 1999; Trager et al. 2000: TFWG00). For instance, even in the simple case of elliptical galaxies, age works in masking possible metallicity effects (Renzini & Buzzoni 1986; Worthey 1994). Since SBF are generated by the poissonian fluctuations of the stellar counts in each pixel of a galaxy image, they have a well understood physical origin (dictated by the properties of the stellar population where they originate from). The amplitude of these fluctuations is determined by the age, chemical composition, and distribution of the evolving stars in the proper evolutionary phases. Thus, theoretical SBF colors and magnitudes are expected to provide a diagnostic of the stellar content of galaxies, useful in decoupling age from metallicity (LCG00, BVA01).

So far, only a handful of theoretical works on the SBF modeling are available (W93; B93; LCG00; BVA01; Mei, Quinn & Silva 2001). In spite of this impressive results, still models based on different ingredients (stellar evolutionary tracks, temperature-color transformations) and detailed assumptions (HB morphology, AGB evolution, mass loss, etc.) are needed in order to compare the various theoretical expectations and thus improve the reliability of the theoretical framework. A lightening example of the present situation is offered by Fig. 5 of LGC02, clearly showing that the inferred ages and metallicities depend on the choice of models.

The presentation of our work is organized as follows. The basis of the model is described in Section 2, where we also present absolute magnitudes and colors for the optical and NIR ground-based and HST filters under different assumptions on the chemical composition and the age. Section 3 reports on a comparison between our SBF predictions and those by other authors. The effects of the Initial Mass Function (IMF) and the contribution of stars in late evolutionary phases are explored in Section 4, together with a discussion on the impact of using different color-temperature libraries. After testing our SBF models as distance indicators on Galactic Globular Clusters (GGCs) and galaxies, in Section 5 they are applied to derive population parameters of some galaxies. Theoretical calibrations are presented in Section 6. The main results are summarized in Section 7.

2. SBF synthetic model

Our SBF model is based on the stellar population synthesis code described and tested observationally in Brocato et al. (1999; 2000: BCPR00). This code is optimized to reproduce both the observed distribution of stars in the color-magnitude diagrams (CMDs) and the integrated properties (color and spectral indices, energy distribution, etc.) of GGCs and galaxies. Here we report the main ingredients used in the present version of the code, referring to the quoted papers for details on the theoretical background.

All the computations refer to Simple Stellar Populations, i.e. single-burst stellar systems with homogeneous chemical composition, and an IMF to be randomly populated by our model machinery (Appendix A). Those models computed by assuming a bimodal Scalo-like IMF in the mass range $0.1 - 1.5\ \mathcal{M}_{\odot}$ will be called **reference models** in the forthcoming.

The database of stellar evolutionary tracks is from the Teramo-Pisa-Roma group, based on the evolutionary stellar code FRANEC (Cassisi et al. 1998, and references therein). Here we include tracks with metallicity ranging from $1/200\ Z_{\odot}$ to super-solar metallicity $2Z_{\odot}$ (Castellani, Chieffi & Pulone 1991; Castellani, Chieffi & Straniero 1992; Bono et al. 1997a, 1997b). These sets of tracks cover all of the major evolutionary phases: main sequence (MS), sub-giant branch (SGB), red giant branch (RGB), He-burning phase (horizontal branch, HB), asymptotic giant branch (AGB). The latest stages, which are crucial for SBF calculations, have been treated with special care; they extend to Post-AGB (PAGB) and white dwarf (WD) sequences when needed.

In each reference model, mass loss along the RGB and AGB is taken into account following the prescriptions by Reimers (1975). In particular, along the RGB we adopt $\eta = 0.4$, which is able to reproduce the typical HB stars distributions and the integrated colors in globular clusters (Renzini & Fusi Pecci 1988; BCPR00). A slightly higher value is taken for stars in the upper part of the AGB ($\eta_{AGB} = 0.8$, see paragraph 4.2.2), which reproduces the observed amount of mass loss of very bright stars (Le Bertre et al. 2001).

The magnitudes of the stars are derived assuming the bolometric corrections and the colors by Lejeune, Cuisinier & Buser (1997, LCB97) for the standard Johnson-Cousins $UBVRIJHK$ photometric system. We provide also SBF amplitudes for a set of HST *WFPC2* and *NICMOS* filters covering almost the same range of wavelengths (namely $F439W, F555W, F814W, F110W, F160W$ and $F222M$), adopting the transformation tables by Origlia & Leitherer (2000, OL00). The effects of other transformation recipes, resting on different assumptions, will be discussed in Section 4.3.

As an example of the color-magnitude diagrams of the SSP under investigation, we plot in Fig. 1 a sample of CMDs for a fixed age t=15 Gyr, and for three chemical compositions ($Z = 0.001, 0.01,$ and 0.02).

The present procedure to derive the SBF differs from the "usual" one, based on the ratio of the second to the first moment of the luminosity function (TS88; W93; Worthey 1994; LCG00; BVA01). Our method is briefly outlined here; a detailed description and a discussion are reported in Appendix A and in Cantiello (2001).

By a Monte Carlo random method, we compute a SSP model with a fixed number of stars N_{star}, for a given set of stellar population parameters: age, chemical composition, IMF, etc.. This provides an integrated flux (F_X) within each specific filter X. The same set of parameters is used to compute N_{sim} independent simulations. The corresponding SBF are explicitly calculated as:

$$\bar{F}_X = \frac{\langle F_X - \langle F_X \rangle \rangle^2}{\langle F_X \rangle} \tag{1}$$

where $\bar{F}_X$ is the flux fluctuation from which we derive the SBF amplitude $\bar{M}_X$.

To match the typical number of stars per pixel in real observations N_{star} is chosen to be $\simeq 10^5$ (e.g. B93). By increasing N_{sim} (to a maximum of 10^5 experiments), the "fluctuations" of $\bar{M}_X$ tend to vanish, i.e. $\bar{M}_X$ tends to an asymptotic value. As an example, Fig. 2 shows the value of the I-band SBF amplitude ($\bar{M}_I$) versus N_{sim} for a model with $Z = 0.02$, $Y = 0.289$ and $t = 15\ Gyr$. For small N_{sim} (say, $N_{sim} \lesssim 500$), $\bar{M}_I$ oscillates strongly. For $N_{sim} > 1000$ simulations, $\bar{M}_I$ approaches the asymptotic value $\bar{M}_I^{asym} \simeq -1.47\ mag$ and keeps well within the best observational accuracy of SBF measurements ($\sim$0.05, T01), i.e. $|\bar{M}_I - \bar{M}_I^{asym}| \lesssim 0.05$. By repeating the same procedure for different sets of the parameters of stellar populations and for different filters, we found that $N^*_{sim} = 5000$ is appropriate to all the photometric bands used here for the adopted $N_{star} \simeq 10^5$.

2.1. SBF versus Chemical composition and age

In order to cover the typical chemical compositions and ages of both GGCs and galaxies, we computed the SBF absolute magnitudes for the following set of chemical compositions: ($Z = 0.0001, Y = 0.23$); ($Z = 0.001, Y = 0.23$); ($Z = 0.01, Y = 0.255$); ($Z = 0.02, Y = 0.289$); and ($Z = 0.04, Y = 0.34$). The values for the ages are $t = 5, 9, 11, 13$, and $15\ Gyr$. The resulting SBF are listed in Table 1 (a, b) for ground-based and HST filters. The complete output of the models (CMDs, integrated colors, and SBF amplitudes) are available on request via web.

Fig. 3 reports the SBF predictions as a function of metallicity. We consider two ages, $t = 15$ and $t = 5\ Gyr$, and both sets of filters (Fig. 3a refers to ground-based, Fig. 3b to HST filters). In the optical range all the SBF amplitudes become fainter with increasing metallicity, while the opposite trend is shown by NIR bands. This behavior does not depend on the age, at least in the range investigated in this paper. Moreover, it supports the conclusion by W93 of the possible existence of an ideal filter centered at $\sim 1\mu m$ that is expected to be independent of metallicity.

For $Z \lesssim 0.01$ the least sensitive band is I; this means that $\bar{M}_I$ is an excellent distance indicator for metal poor old stellar systems. At higher metallicities ($Z \gtrsim 0.01$) the slope of the relation $\bar{M}_X$ versus Z increases for all the SBF amplitudes and is similar for all bands ($BVRI$) but for U. In general, $\bar{M}_U$ has a quite different behavior in the whole range of metallicity, varying of $\sim 3.2\ mag$ due to the strong decrease of the U mean luminosity of the brightest stars in the population as the metallicity increases (Fig. 1). Although ruling out $\bar{M}_U$ as a reliable distance indicator, this high sensitivity makes it an excellent population tracer. Unfortunately, no SBF measurements are available in the U filter so far. The predicted small variations of JHK bands at $Z \gtrsim 0.01$, coupled with high luminosity, support the increasing number of SBF measurements in these bands. The SBF amplitudes computed for the HST filters (Fig. 3b) show a behavior quite similar to the corresponding ground-based filters.

The next step is to understand the effects of variations in the age of the stellar population on the SBF amplitudes. The results of our computations for models of age t =5, 9, 11, 13, 15 Gyr are

plotted in Fig. 4 for both a metal-rich ($Z = 0.02$), and a metal-poor ($Z = 0.0001$) stellar system. In general, the sensitivity to age grows from U to I, with changes remaining below ~ 0.4 mag. JHK bands are more sensitive; SBF amplitudes increase by about 0.7 mag from 5 to 15 Gyr, in agreement with BVA01 and LCG00. However, for stellar populations with age in the range under consideration, JHK SBF are strictly dependent on the adopted treatment of the brightest evolutionary phases (thermal pulses, mass loss processes, etc.), as we will show in Section 4.2.

Let us finally remark that the SBF amplitudes for old stellar populations are much more sensitive to metallicity changes than to age, particularly at optical wavelengths. A similar conclusion, even with slightly different absolute SBF values, has been reached by other authors (B93; LCG00; BVA01), who adopt different approaches and ingredients to derive population synthesis models. In this sense this result may be regarded as theoretically well established, i.e. it does not depend on the adopted stellar population models.

3. Comparisons with other models

We compare our work with the models by BVA01 and LGC02. Since the grids of ages and metallicities do not match, for the comparison we select the values as similar as possible. We restrict the discussion to populations of fixed age ($t \sim 15$ Gyr), and to V, I, $F160W$ photometric bands. Fig. 5 plots the SBF predictions versus the $(V-I)_0$ (*Right panel*) and $[Fe/H]$ (*Left panel*) for single-burst stellar population models.

In spite of the very different theoretical framework, the general trends of the SBF amplitudes versus both metallicity and the integrated $(V-I)_0$ color are the same for all authors. However, for metallicity higher than solar, BVA01 and LGC02 predict fainter SBF amplitudes in V and I bands (up to ~ 0.5 mag) and a similar, but less relevant, difference appears in the $F160W$-band.

The reasons for such a discrepancy are expected to be in the basic ingredients and in the transformation tables. Our models are based on a completely different evolutionary framework compared to BVA01 and LCG00, whose models rely on the Padua stellar evolution database, although they use two different compilations of isochrones (Bertelli et al. 1994, and Girardi et al. 2000 respectively), and different prescriptions for the AGB stars. Furthermore, we adopt a different approach to populate the brightest evolutionary phases (HB, AGB, thermal pulses) as we shall show in the following Sections. For an extensive discussion on the impact of evolutionary tracks and transformations tables on SBF expectations, the reader may refer to LCG00 and to our Section 4.3.

Let us remark that there is a substantial difference in the meaning of the two panels of Fig. 5: $[Fe/H]$ is an input parameter for all the models, so it is directly comparable, while the $(V-I)_0$ color is an output of each code, then it depends on the adopted evolutionary tracks, on the procedure in populating the isochrones, and so on. Obviously, it may vary from model to model even for the same input parameters.

4. On the assumptions of the reference models

Starting from the reference models, in this Section we investigate the sensitivity of SBF to IMF, late evolutionary phases, and color-temperatures relations.

4.1. Initial Mass Function

Usually the mass spectrum of a stellar population is described by the simple power law proposed by Salpeter (1955) or by the bimodal (or more) function of Scalo (1986 and thereafter). Indeed, a crude extrapolation of the Salpeter law to masses $\mathcal{M} \lesssim 1\mathcal{M}_{\odot}$ seems to fail, while the flattening and even possible declining behavior of the Scalo IMF appears more appropriate. For these reasons, in our reference calculations we have adopted a Scalo-like IMF. Nevertheless the slope of this function at the lowest masses still remains very uncertain (Reid 1998). In this Section we evaluate the contribution to the SBF by the lowest mass stars, and what happens under significant changes in the slope of the IMF. Two different numerical experiments are performed on an old solar-metallicity SSP ($t = 15\ Gyr$, $Z = 0.02$, $Y = 0.289$):

a) SBF amplitudes are computed for a set of models obtained by adopting an IMF starting from different low mass limits, namely $\mathcal{M}_{low}$=0.85, 0.6, 0.4, and 0.1 $\mathcal{M}_{\odot}$, by keeping constant the number of RGB stars (actually ~ 100). For all these simulations we adopt a Salpeter-like slope ($x = 1.35$) in order to enhance the contribution of very low mass stars (Table 2).

The table shows that the SBF amplitudes increase with the mass limit $\mathcal{M}_{low}$, the differences being fairly negligible or small in all cases but in the interval $0.6 - 0.85\mathcal{M}_{\odot}$, whose upper limit is of the order of our Turn-Off Mass ($\mathcal{M}_{TO}$, in the model quoted here $\mathcal{M}_{TO} \simeq 0.90\mathcal{M}_{\odot}$). As a matter of fact, the ignorance of the upper part of the MS ($\mathcal{M}_{TO} - \mathcal{M} \leq 0.25\mathcal{M}_{\odot}$) leads to underestimate the total luminosity of the population, which is obviously relevant in computing SBF because it represents the denominator of eq. 1. On the contrary, to add MS stars with $\mathcal{M} < 0.6\ \mathcal{M}_{\odot}$ causes small variations of the SBF, since the total luminosity of the stellar population does not change significantly. Note that this is true even though stars with $\mathcal{M} < 0.6\mathcal{M}_{\odot}$ represent nearly 90% of the total number of stars in the population. In conclusion, no matter how (reasonable ways) the mass spectrum at $\mathcal{M} < 0.6\ \mathcal{M}_{\odot}$ is chosen, its contribution to SBF will not exceed 0.1 *mag* in the most sensitive band K.

b) The effect on the SBF values due to the IMF slope is explored by varying the exponent of the power law (x=0.35, 1.35, and 2.35) for masses $\mathcal{M} > 0.4\ \mathcal{M}_{\odot}$ and assuming a flat distribution for masses $\mathcal{M} < 0.4\ \mathcal{M}_{\odot}$ (Table 3). Not surprisingly the variations are rather small ($\Delta\bar{M}_X \lesssim 0.2\ mag$); x affects mainly the number of the MS stars, which in turn affect only slightly the predicted SBF amplitudes, as previously shown. However, an increased/decreased number of post-MS stars is foreseen if the exponent has a lower/larger value than the Salpeter's one. Since the fluctuation rests mainly on the RGB stars, this explains why SBF brighten with decreasing IMF exponents,

and viceversa.

We conclude that variations on the IMF slope and/or the contribution of low mass stars to the SBF amplitude, *although not negligible*, play a secondary role with respect to the quantities (and assumptions) affecting the post-MS evolution, as for example the chemical composition and age of the populations. The result obtained with our new and fully independent code strengthens what originally found by W93, and recently confirmed by other authors as well (e.g., BVA01).

4.2. SBF versus brightest stars

As just recalled, the SBF signal is very sensitive to the properties of the most luminous stars of the stellar population, as it is the ratio of the second to the first moment of the stellar luminosity function. This requires the SSP models to reach a high level of accuracy in reproducing the post-MS evolution. Therefore, one of the aims in optimizing our code has been to fine-tune the stellar counts during the latest and fastest phases experienced by low mass stars along their evolution (see also BCPR00).

Below we discuss the expected SBF sensitivity to the very bright stars in post-MS evolutionary phases: HB morphology, thermal pulses (TP), and PAGB phases.

4.2.1. Horizontal Branch Morphology

As well known, the main parameter regulating the HB morphology of a generic stellar population is the metallicity (Lee, Demarque & Zinn 1987). If one considers just the effect of Z, the expected HB morphology is that of Fig. 1: *blue* or *intermediate* for $Z \lesssim 0.001$, *red* when $Z > 0.004$. Thus, the distribution in color of low mass stars during the central He-burning stage is expected to play a major role in predicting UB SBF (see also W93). This is particularly true for high metallicities since the HB stars become brighter than the RGB tip (Fig. 1).

Although we shall not discuss the nature of the second parameter (Freeman & Norris 1981), our models take into account that the metallicity is not the only quantity which can affect the HB morphology. Here, we adopt the HB morphology as directly produced by metallicity and by mass loss along the RGB (i.e. we use the mass loss to simulate the effect of the second parameter whatever its real nature is). Along the same vein, one may recall that mass loss during the RGB evolution controls the actual total mass of the HB star and then affects its location in the CMD (Rood 1973). Moving from low to high values of mass loss, the total mass of the HB stars decreases; this fact implies, on average, higher temperatures and bluer colors. On the observational side, there are indications of mass loss enhancement for increasing values of metallicity (e.g. Kudritzki, Pauldrach & Puls 1987).

On this basis, we have investigated the importance of HB morphology on SBF by simulating

different amounts of mass-loss along the RGB, i.e. we have changed η in the Reimers formula ($\eta = 0.2, 0.4, 0.6$, and 0.8) in computing a set of SSP models with given metallicity ($Z = 0.01, 0.02$, and 0.04) and age ($t = 15\ Gyr$).

Table 4 summarizes the SBF values for all ground-based filters. The effects on $UVIK$ bands SBF amplitudes are shown in Fig. 6. The growth in luminosity of U-band SBF and the constancy of the other optical bands confirms the above expectation. We note that the effect is more pronounced for $Z = 0.01$ ($\Delta\bar{M}_U \sim 2\ mag$). For this metallicity, an enhancement of the mass loss on the RGB reduces the mass of the "forthcoming" HB stars by a quantity large enough to populate the blue side of the HB. The larger is the mass loss, the larger is the number of blue HB stars and, consequently, the larger is the U-band SBF amplitude. For higher metallicity systems, variations are still present but of smaller amplitude ($\Delta\bar{M}_U \sim 0.5\ mag$) just because the mass of the RGB stars for the selected age is so large that only red HB stars are produced even for the largest mass loss rates considered here.

From Fig. 6 it is also apparent the opposite behavior shown by $\bar{M}_K$ which depends on the fact that, as η increases, the number of bright stars evolving on the AGB is smaller.

Let us note here that an age of 15 Gyr is selected because models with younger ages provide a red clumpy HB morphology independently of any reasonable value of the η parameter. This is because, by decreasing the age, the HB is populated by stars of increasing mass, which spend their He-burning phase at the red portion of the HB. Thus, no changes are expected on SBF. An unlikely value of $\eta \sim 2.0$ along the RGB phase would be needed to force the models to a blue HB morphology. However, this extremely high mass loss on the RGB would imply a similar (or larger) efficiency along the AGB. This means that the stars are expected to lose their H-envelope, and quickly move to the WD cooling sequence during the very early part of the AGB ascension. Such an improbable scenario leads to SBF which are found to be fainter, particularly for the redder color (up to 1 mag for the K-band), when compared to models with more realistic assumption on the RGB mass loss efficiency.

The present results, even if they do not provide an exhaustive picture of the problem, give quantitative indications on the U and B bands SBF variations as a function of the HB morphology. The effect of η on SBF was also explored by B93, but his synthetic models have always a red clumpy HB morphology for populations with $Z > 0.001$.

We conclude that changes in the HB morphology, as induced by reasonable assumptions on the mass loss along the RGB, have a negligible impact on SBF, if one considers filters redder than B.

4.2.2. Thermal Pulses

Mass loss strongly affects the He-exhaustion stages too, and determines different scenarios for the evolution of stars leaving the HB, either to the TP phase or rapidly to a PAGB condition. According to the observations (e.g. Alard et al. 2001), mass loss becomes more and more efficient as the star climbs the AGB, till the ejection of the stellar envelope during the last superwind stages (Renzini 1981).

To extend our He-burning evolutionary tracks to the TP phase, we follow the prescriptions by Groenewegen & de Jong (1993) as in a previous paper (BCPR00). As cited above, our reference models simulate the mass loss process along the AGB by adopting an enhanced Reimers coefficient η (namely $\eta_{AGB} = 0.8$). The corresponding mass lost by stars is in the range from 10^{-7} to $10^{-6}\mathcal{M}_{\odot}\ yr^{-1}$, in fair agreement with observations of AGB stars (e.g. Le Bertre et al. 2001).

If the age of the population is fixed, an increase of the mass loss rate reflects into a decreasing of the number of very bright AGB stars just because their H-rich envelopes become quickly so thin that the stars leave the AGB phase. According to this simple view, an increase of the mass loss rate induces a corresponding decrease of the foreseen luminosity of the AGB tip. This occurrence has to affect SBF amplitudes. To investigate such an issue quantitatively, we computed a series of SBF models by changing η_{AGB} from 0.4 to 3.2. The results in the Johnson-Cousins filters are reported in Table 5 for solar metallicity and the labeled ages. Dealing with AGB stars, the effect is more remarkable in the redder bands. Fig. 7 illustrates the SBF dependence on η_{AGB} for models with different ages and solar chemical composition in the $IJHK$ filters.

Such a dependence provides the unique opportunity of using the SBF to constraint evolutionary parameters during the late stage of the AGB and TP phase. In particular, we calibrate the mass loss efficiency along the AGB. Each panel of Fig. 8 shows the I-band SBF predictions computed with a specific value of η_{AGB} (0.4, 0.8, 1.6, 3.2). To perform this calibration we use the mean empirical relations $\bar{M}_I$ versus $(V-I)_0$ as derived from observations of galaxies and GGCs. The inclined solid line in the range $1.0 \lesssim (V-I)_0 \lesssim 1.3$ represents the relation derived by T01. According to T01 the slope of this relation is quite well established, whereas the zero point is more uncertain with a rms scatter as large as 0.1 *mag* (see Table 4 in TBAD97). However, the true indetermination of the zero point is expected to be of the order of 0.20 *mag*, since one has to include the uncertainties in the Cepheid zero point (Mould et al. 2000, Freedman et al. 2001) and in the LMC distance modulus (e.g. Benedict et al. 2002). The horizontal solid line in the range $0.8 \lesssim (V-I)_0 \lesssim 1.0$ refers to the observed locus of GGCs (Ajhar & Tonry 1994: AT94), after a recalibration according to BVA01 prescriptions (eq. 5 in BVA01). In this case the quoted rms scatter is ~ 0.25 *mag*. In addition, the zero point of the horizontal line has an indetermination of at least $0.1 - 0.15$ *mag* arising from the uncertainty of the GGCs distances.

Fig. 8 shows that the two extreme values of the η_{AGB} do not match the observed SBF. In fact $\eta_{AGB} = 0.4$ provides too bright SBF amplitudes at all metallicities but $Z = 2Z_{\odot}$; on the contrary, the models with $\eta_{AGB} = 3.2$ appear definitively fainter than observations. The intermediate cases

are more interesting: both the η_{AGB} values fairly reproduce the SBF data. However, the horizontal line representing the GGCs measurements is fitted by SBF simulations of the proper metallicity values but of quite different ages. The assumption of $\eta_{AGB} = 0.8$ leads to a remarkable fit with models of $13 - 15\ Gyr$, while $\eta_{AGB} = 1.6$ requires an age of the order of $\sim 9\ Gyr$. Since our SSP models reproduce the CMDs and integrated properties of GGCs when an age of $\sim 15\ Gyr$ is assumed (BCPR00), we find that $\eta_{AGB} = 0.8$ simulates the mass loss process on AGB in such a way that the resulting distribution of stars on the AGB is able to reproduce at the same time the SBF measurements in galaxies and in GGCs.

In spite of the large uncertainties on the zero points, this result represents a relevant constraint for stellar evolution models of AGB stars. Even if the exact values of η_{AGB} depend on the assumed theoretical framework, the method outlined here remains a new and powerful tool to improve our knowledge on the details of the evolution of AGB stars.

4.2.3. Post-AGB stars

The theory predicts a small number of PAGB stars (Renzini 1998, BCPR00) which, however, increases with the total number of stars. Though rare objects, PAGB stars cannot be ignored when dealing with populous systems such as galaxies (Greggio & Renzini 1990; Brocato et al. 1990).

For the complex evolution off the asymptotic branch we rely on the stellar models by Vassiliadis & Wood (1994, VW94) and Blöcker & Schömberner (1997, BS97). Since SBF are sensitive to the most luminous stars, as first approximation, we simulate only the most luminous PAGB, neglecting Post-Early-AGB evolved stars, which leave the Hayashi track at lower luminosity before the first thermal pulse (Castellani & Tornambè 1991). Under these assumptions, we computed SBF amplitudes for the reference stellar populations with solar metallicity and $t = 15\ Gyr$, by simulating a different amount of PAGB stars (N_{PAGB}) for the same total number of stars. To perform these simulations, firstly we evaluate the number of PAGB with respect to the number of expected HB stars (N_{HB}) by following the prescriptions by BCPR00. Secondly, we explored a wide range of values of N_{PAGB}/N_{HB} by artificially varying this ratio.

In Fig. 9 we plot the UBV and I bands SBF amplitudes versus the ratio N_{PAGB}/N_{HB}. The shadowed region corresponds to the value of N_{PAGB}/N_{HB} properly derived according to BCPR00. It is apparent that SBF obtained in filters redder than V are not affected by the presence of bright PAGB stars. On the other hand, U and B SBF appear to be quite sensitive to the number of predicted PAGB stars, independently of the assumed stellar evolutionary tracks (VW94, BS97). Here, we suggest that precise measurements of U and B SBF, with telescopes having a high efficiency at such wavelength (for example the VLT Survey Telescope, or VST: http://twg.na.astro.it/vst/vst_homepage_twg.html), would provide the unique chances of deriving valuable constraints to stellar evolution theory of PAGB stars.

Finally, we find that the luminous and hot stars crossing the CMD from the AGB tip to the

beginning of the WD cooling sequence do not appreciably affect the SBF amplitude in most of the bands but U and B. We also note that the stars evolving down along their WD cooling sequence are not expected to provide a significant contribution in optical bands. In fact, it becomes more and more negligible as the WDs luminosity decreases, even though they pile up due to longer evolutionary times.

4.3. Impact of Atmospheres transformations

The relations transforming the theoretical quantities ($log\ L/L_{\odot}$ and $log\ T_{eff}$) into observables (magnitude and colors) are of fundamental importance in modeling SBF. In general, theoretical relations between colors/bolometric constant and temperatures suffer from the complexity in treating molecular and atomic transitions when the metal content increases and the star temperature decreases. When the metal content grows up to solar or super-solar values, these difficulties become more and more severe due to the formation of grains and complex molecules in the outer part of the atmosphere, which cause strong blanketing effects (Bell 1973). On the other hand, empirical compilations involve difficulties in deriving fundamental star parameters as metallicity and gravity from observed spectra and colors (Alonso, Arribas & Martinez-Roger, 1996, 1999).

In this Section we evaluate how SBF amplitudes change by adopting different transformation tables available in literature. To provide a quantitative comparison we selected three color-temperature compilations commonly used for synthetic stellar population models: the theoretical tabulation by Castelli, Gratton & Kurucz (1997: CGK97), the hybrid library by LCB97, and the semi-empirical Yale transformations (Green et al. 1987: G87). The CGK97 tabulation is the result of the atmosphere models obtained with the updated Kurucz's code. LCB97 corrected tabulations are based on the theoretical spectra from different authors, properly adapted to match observations (see LCB97 for more details). The semi-empirical tables proposed by the Yale group result from the calibration of the old Kurucz models (1979). Both CGK97 and LCB97 include all the ground-based Johnson-Cousins filters ($UBVRIJHK$), while G87 tables cover only the optical range ($UBVRI$).

We computed a set of stellar population models for the selected metallicities, $t = 15\ Gyr$, and with the reference assumptions on mass loss and IMF. For each model we evaluated SBF amplitudes by adopting all the three tabulations mentioned above.

The results are reported in Table 6. The relative differences in the SBF amplitudes for selected filters ($UBVRIJHK$) are plotted in Fig. 10 as a function of the population metal content, Z, for a fixed age. The differences are computed relatively to LCB97. For $Z < 0.01$ Fig. 10 shows that SBF amplitudes are quite well determined. In this metallicity range (GGCs) there are differences $\lesssim 0.2\ mag$ by using either CGK97, or LCB97, or G87; a fact supporting the reliability of SBF models of these metallicities.

The situation worsens for higher metallicities. For $Z > 0.01$, G87 transformations lead to systematically brighter SBF amplitudes in all the considered bands (up to more than 1 mag for

the I-band). Such a large difference may be due to the fact that G87 transformations have been calibrated with GGCs, which are low metallicity objects. LCB97 and CGK97 models give quite similar predictions for all the optical and NIR bands. Sizeable differences are only expected in V and R bands, where the SBF are about 0.3 *mag* brighter in CGK97 models.

In order to understand the origin of these differences we show the color-magnitude location of the most luminous stars of a solar-metallicity isochrone aged 15 *Gyr* transformed by adopting all the quoted compilations. For clarity, we focus the attention on RGB stars, bearing in mind that AGB stars behave similarly. We consider as representative the (M_V, $(V-I)_0$), (M_I, $(V-I)_0$), and (M_K, $(V-I)_0$) diagrams in Fig. 11. The isochrone mapped in the observational plane by using G87 provides a much brighter RGB tip (where stars reach temperatures lower than 3500 K) in the I-band (Fig. 11 middle panel) with respect to LCB97 (and CGK97); this could explain the brighter I-band SBF amplitude obtained by using G87. Moreover, since the tip magnitude calculated with LCB97 is fainter than those with CGK97 for all bands, one expects SBF to become fainter and colors redder for metallicity higher than solar when LCB97 is adopted, as exactly shown by Fig10.

In Fig. 11 we also plot the isochrone transformed with the empirical temperature-color relations published by Alonso et al. (1996, 1999), since they are used in BVA01 SBF models. We note that RI filters involved in the Alonso et al. transformations are the Johnson & Morgan (1953) bands, with respect to the Cousins (1976, 1978) passbands commonly used for SBF observations. By applying the relations to convert $(V-I_J)$ into $(V-I_C)$ (in Fig. 11 we used Bessel 1979), the differences become negligible, making Alonso et al. models similar to the others in their own temperature range. A significant disadvantage of this grid is that it is limited to $T_{eff} \geq 3750$ K for $[Fe/H] > -1.0$, then one needs to extrapolate or to merge with other tables down to lower temperatures. For all these reasons we decided not to use these color-temperature relations in computing SBF.

5. Comparison with the observational data

As a first step we compare our SBF predictions in several bands with actual observations of stellar systems (GGCs and galaxies) with known distances. Then, the theoretical SBF are used to derive the characteristics of a selected sample of observed stellar populations.

5.1. Galactic Globular Clusters

The only SBF measurements related to GGCs are those by AT94 for a sample of 19 objects. There are several reasons to study the SBF of these objects: 1) GGCs span a range in metallicity down to values lower than expected in galaxies; 2) since they are thought to be formed by the gravitational collapse of a homogeneous gas cloud, they are the best observational counterpart of theoretical SSPs; 3) the SBF of GGCs are determined directly from their resolved stars (differently

from galaxies, which require a more complex analysis). Thus GGCs SBF represent a simple and unambiguous target to verify the stellar evolution assumptions.

Before going on, it is worth noticing that, since the amount of stars in a globular cluster ($10^5 - 10^6$) is far lower than the stellar content in a typical galaxy ($> 10^{10}$), this might bear on the SBF evaluations due to statistical reasons. Consequently, the proper way to evaluate theoretical SBF for GGCs is to compute simulated CMDs (with total number of stars $N_{star} \sim 10^6$) and apply directly the equations $7 - 9$ of TS88. In spite of the difference in the total number of stars, the resulting SBF are quite similar (within the uncertainties) to the values for $Z \leq 0.006$ derived from the procedure presented in Section 1 (Table 1). Such a stability in the computed SBF amplitudes is due to the compensation of two conflicting effects, which arise when the size of the simulated stellar population decreases. On one side, the number of stars expected in the fastest and brightest evolutionary phases (e.g. TP, AGB) tends to vanish, and fainter SBF amplitudes are obtained. On the other side, the number of bright RGB stars decreases providing less populated RGB; statistical effect become relevant (see also BCPR00), leading to brighter SBF amplitudes.

Since AT94 measurements are available only for VI bands, the comparison with theoretical models can be done only for these two filters. In Fig. 12 the GGCs observational data are compared with our models. The observational absolute SBF magnitudes for each globular cluster are obtained from the AT94 data according to the expression: $\bar{M}_X = \bar{m}_X - DM$, where DM is the distance modulus. The latter quantity, the metallicity, and other properties are from the latest version of the electronic catalog compiled by Harris (1999), and are summarized in Table 7, which also reports the observed SBF values. In the figure the solid (long-dashed) line connect the oldest (youngest) models with different metallicity. The dotted lines represent the mean line according to BVA01 prescriptions (their eq. 5). From Fig. 12 it is apparent that:

i) the DM directly derived from the theoretical SBF are in very good agreement with the recent evaluation from other distance indicators;

ii) the general trend of observed SBF versus metallicity is well reproduced by theoretical models; this fact is noteworthy because the $[Fe/H]$ values of GGCs are measured directly and not just derived by integrated colors.

Finally, let us note that the good agreement between the single measurements and the models is particularly relevant considering that no effort has been put in reproducing the peculiarities of each individual GGC (e.g. HB morphology, brightest stars, etc.).

5.2. The Galaxy sample

Unfortunately, no GGC with $Z \gtrsim Z_\odot$ is known, and one needs to look at elliptical galaxies and bulges of spirals to verify the degree of accuracy of SBF predictions for metal rich populations.

For this purpose, we extract a subsample of galaxies from the T01 I-band database by selecting

objects with reliable distance estimates as derived by Ferrarese et al. (2000). The result is given in Table 8, where data of 31 galaxies are summarized. In the table we report from left to right: the galaxy name, the morphological type T, the visual absorption A_V, the integrated color $(V-I)_0$, and the SBF apparent magnitudes in $I, V, R, K', K_s, F814W$, and $F160W$ filters. The last column reports the galaxy distance derived from Cepheids, when available (8 galaxies), otherwise the average distance from other indicators (Ferrarese et al. 2000). We note that, for the sample of galaxies with Cepheid-based distances, the new calibrations of the Period-Luminosity (PL) and Period-Luminosity-Metallicity (PLZ) relations by Freedman et al. (2001) lead to DM which differ on average of $\Delta DM_{PL} = 0.13 \pm 0.06$ and $\Delta DM_{PLZ} = 0.03 \pm 0.05$, respectively. Being the debate on PL and PLZ still open, we adopt the Ferrarese et al. database for sake of homogeneity and clearness.

We test the consistency of our predicted SBF starting from galaxies with distances evaluations based on Cepheids, as they are the most reliable distance indicator. Since the SBF method works at its best with spheroidal galaxies, there is a relative scarcity of SBF measurements for spirals, and even less objects with both SBF and Cepheids distance determinations. We first focus the attention to the I-band, due to its importance for the calibration of the empirical relation (T01), and then we extend the analysis to other photometric bands. Fig. 13 illustrates the comparison of the sampled galaxies with the present models; the empirical line by T01 is also plotted. The figure shows that all the galaxies well match the theoretical models with $(V-I)_0 > 1.0$ *mag*. We emphasize that the zero point of the empirical relation by T01 is derived directly from Cepheids-calibrated distances, while the present theoretical SBF are completely independent of them. At $(V-I)_0 < 1.0$ the theory predicts a nearly constant value of I-band SBF for models of similar age, as already verified on GGCs measurements. Moreover, this appears in agreement with the location of the galaxy NGC 5253 (not plotted in the figure) reported in Fig. 8 by BVA01.

By extending the comparison to all the galaxies in Table 8 (Fig. 14), the agreement remains good, even if few of the observed values appear fainter than those predicted by the theory and by the empirical line. We note that the galaxies showing the largest scatters (NGC 4278 and NGC 4565) have distance measurements with a quite large spread, if compared to internal uncertainties (Ferrarese et al. 2000).

Taking advantage from multi-band observations, in Fig. 15a,b,c we report a similar comparison for V, K, and $F160W$ filters. Following Jensen et al. (2001) we discard NGC 4536 from their sample because its anomalous $F160W$-band SBF magnitude appears to be due to clumpy dust contamination. Fig. 15 shows that our theoretical predictions are consistent with observations not only in the I-band, but also in other selected optical and NIR filters. This result is relevant for two reasons. First, the agreement of absolute values of the SBF amplitudes suggests that the present theoretical SBF, computed in the other selected photometric bands, may be adopted to derive distances too. Second, the agreement over a wide range in wavelength supports the reliability of the global theoretical assumptions on the stellar population from which we derive the SBF.

Being the proposed theoretical framework supported by SBF observations, at least in the main relevant features, we are led to push forward the capability of the SBF technique and to tentatively infer information on age and metallicity from the SBF measurements of the quoted sample of galaxies.

5.3. SBF as Stellar Population tracers

Once the distance of an object is known or in the case of several objects all at the same distance (e.g. cluster galaxies), one may want to use the SBF models for deriving ages and metallicities of the stellar populations. To this end we test here the internal consistency of the SBF models in various bands, basically V, I, K and $F160W$. As further point we verify the reliability of the inferred (average) age and metallicity through the comparison with literature values derived by other methods.

The problem of evaluating the age and metallicity of stellar populations in elliptical galaxies is a largely debated topic (see for example Henry & Worthey 1999 and reference therein). Thus, to select measurements or evaluations of those quantities which can probe the reliability of SBF models in deriving t and Z is a quite a difficult step. For example, one has to face with the problem that ellipticals are constituted by complex stellar populations, i.e. by age/metallicity mixed populations (e.g. Baugh, Cole, Frenk 1996; Kauffmann & Charlot 1998; Saglia et al. 2002), while we use the approximation of single-burst stellar population. Another difficulty comes from the evidence that metallicity and/or age gradients are observed in some ellipticals (Peletier et al. 1990; Carollo, Danziger & Buson 1993, Kobayashi & Arimoto 1999). As a further complication SBF measurements and t, Z evaluations from other indicators may refer to not-overlapping regions of the studied galaxy.

Keeping in mind the quoted (relevant) warnings, it is still interesting to evaluate ages and metallicities from SBF measurements by using the present theoretical models. Clearly, the following results refer to SBF measured in relatively extended galaxy regions, and they are valid in the approximation that in these regions there is a dominant stellar population (Ferreras, Charlot & Silk 1999). For all these reasons the comparison between our predictions on t, Z, and those obtained using other methods have to be considered with caution, and within the quoted approximations. The age and metallicity we derive have large uncertainties as expected from the quoted limitations. A more detailed investigation is out of the aim of this paper and it should rely on mixed populations models, and also on SBF measurements for which the radial distribution is known (e.g. Sodemann & Thomsen 1995).

In order to test our ability of predicting age and metallicity, we built a sample of 15 galaxies for which these quantities have been given by other authors (Table 9). Most of these objects come from the compilation by TFWG00 and by Terlevich & Forbes (2002: TF02), who used H_β, $Mg\ b$, and $\langle Fe \rangle$ line strengths to derive age and metallicity for a large sample of elliptical galaxies (see

the quoted papers for more details). These estimations are derived from observational data taken at smaller radii with respect to SBF measurements (except in the case of Jensen et al. 2001, 2003). In addition, TFWG00 find indications of age and metallicity gradients (see their Tables 6A and 6B).

To start with, let us to use the model sequences in the $\bar{M}_X$ versus $(V-I)_0$ plane as already shown in Fig. 14 and Fig. 15. The clear separation between models with low ($Z = 0.0001, 0.001$) and high metallicity ($Z = 0.01, 0.02, 0.04$) for all the explored values of age confirms that this kind of diagrams are a powerful tool for this purpose (see also BVA01, LCG00). Since we are dealing with absolute SBF amplitudes, a particular care has to be taken in selecting the distance moduli required to translate the observed apparent SBF values. Obviously, Cepheids distances are preferred; when they are not available for a single galaxy, we use group-averaged distances. To avoid circular arguments, we recomputed the group distance moduli by Ferrarese et al. (2000) excluding SBF-derived distances, i.e. averaging on the Cepheids, PNLF and TRGB distances. The results are reported in Table 9 for the 15 galaxies. As already stated, Freedman et al. (2001) revised the Cepheids distance scale, and Ciardullo et al. (2002) recently recalibrated the zero point of the PNLF. These new results decrease the group-averaged distances of about 0.14 *mag* if the Cepheid PL relation is used, but they leave nearly unchanged the above determinations when the PLZ is considered.

Fig. 16 displays the theoretical models and the observational data in selected photometric bands. As a first general result, we find that the location of the bulk of galaxies is almost consistent in all the photometric bands. Then we focus on two well studied galaxies: NGC 224 (M31) and its dwarf companion NGC 221 (M32). They have accurate distances and different morphological types, thus they are good prototypes for our investigation.

NGC 221: the observed $V, I, K, F160W$ bands SBF are well reproduced by SSP models with an age between 5 and 9 Gyr and a nearly solar chemical content. These results are very similar to those found by TFWG00 and TF02, i.e. $t = 4.9 \pm 1.3\ Gyr$ with $[Fe/H] = -0.01 \pm 0.05$, and $t = 3.8\ Gyr$ with $[Fe/H] = -0.04$, respectively.

NGC 224: $V, I, F160W$ bands SBF data of the bulge of this galaxy are consistent with SSP models of fairly old age ($t \sim 15\ Gyr$) and solar metallicity. This is in agreement with Bica, Alloin & Schmidt (1990) and Davidge (2001), who find that the bulge of this galaxy is dominated by an old population with metal content $-0.5 < [Z/Z_\odot] < 0.0$. There is a discrepancy with TF02 age estimation ($t \sim 5\ Gyr$). However, Davidge (1997) finds evidence for an age gradient in the center of NGC 224 with an intermediate age population which is probably more concentrated in the center with respect to the main body of the bulge; such population should contribute only for a small fraction (10-20%) to the total visible flux.

It is difficult to derive information from the K-band SBF, due to the already quoted overlap of the models. However, the $\bar{M}_K$ data are consistent with the (t, Z) values inferred from V and I bands estimations. Some remarkable indications on NIR data can be found by comparing the

SSP models which reproduce the V, I bands SBF with the work by Davidge (2001). Observing the brightest AGB stars in M31 bulge, he finds that the bulk of these stars has $K \simeq -8.4\ mag$. By adopting in our SSP models ($t = 15\ Gyr$, $Z = Z_{\odot}$) the mass loss calibration suggested in paragraph 4.2.2 (i.e. η_{AGB}=0.8), we find that the tip of the AGB is as bright as $K \simeq -8.2\ mag$, a value which is in very good agreement with the observational results by Davidge.

Among the other galaxies, here we discuss some examples which support the consistency of our estimates in the various bands and that they are concordant with values proposed in the literature (see Table 9).

NGC 891: it is the most metal poor galaxy in our sample. We derive $Z \sim Z_{\odot}/2$ and age $11 - 13\ Gyr$;

NGC 1316: the $V, I, F160W$ bands SBF magnitudes suggest a young age ($t \sim 5\ Gyr$) and a nearly solar metallicity;

NGC 3377: from V, I-band SBF measurements it appears to be consistent with a nearly solar composition and relatively young age ($\sim 5\ Gyr$);

NGC 3379: an age of the order of $11 - 13\ Gyr$ and a solar chemical composition is derived from the SBF measurements in two bands ($K, F160W$). On the other hand, V and I-band SBF data would require a somehow younger age ($\sim 5 - 9\ Gyr$) and a higher metallicity ($Z > Z_{\odot}$). Such discrepancy will disappear later on, using SBF-color data;

NGC 4382: only SBF measurements in the I-band are available and it seems to be located slightly out of the models grid, in the area of the diagram where we expect to find stellar systems with $Z \gtrsim 2Z_{\odot}$ and age younger than 5 Gyr;

NGC 4472: $I, F160W$ bands SBF measurements are in agreement with an SSP computed assuming $Z = Z_{\odot}$ and old age ($\sim 15\ Gyr$), while a slightly higher metallicity and lower ages are suggested by V and K bands.

For some galaxies the slight discrepancies in the values derived from different bands could be related to the high uncertainty of their distance moduli, coupled with a different sensitivity of SBF in each band to age and metallicity. Concerning distances, we mention also the case of the galaxy NGC 4649, which is located out of the grid of models in the $\bar{M}_I$ panel. As discussed by Ferrarese et al. (2000) the NGC 4649 Virgo-subcluster is not a well defined physical association of galaxies, thus probably the group distance reported in Table 9 is not an appropriate choice for the actual distance of the galaxy. A direct measure of the distance of NGC 4649 comes from PNLF; if we adopt this value the inferred age and metallicity are estimated to be $t \sim 5 - 9\ Gyr$ and $Z = 2Z_{\odot}$. However, we recall that Jacoby et al. (1992) and recently Ciardullo et al. (2002) remark that the PNLF distances seem to be systematically shorter than SBF distances. For this reason we do not report the last estimations in Table 9.

We obtain a discrepancy in the age and metallicity derived from $\bar{M}_I$ and $\bar{M}_{F160W}$ for NGC

4278 and NGC 3384. For NGC 4278 the situation is similar to that of NGC 4649; for NGC 3384 such discrepancy could be related to the multi-component structure of this galaxy (Busarello et al. 1996), coupled with the fact that HST SBF measurements refer to the very inner region of the galaxy while an outer region is observed by T01.

The above results are summarized in Table 9 (columns 7–8). Clearly, the comparison with TFWG00 and TF02 evaluations should not be over-interpreted; nonetheless the fair agreement obtained is remarkable and supports the reliability of our models.

Although $\bar{M}_X$ versus $(V-I)_0$ planes can be used to set useful (though not stringent) constraints to the evolutionary properties of the main stellar population present in a galaxy, the drawback is mainly the dependence on the adopted distance and on the partial degeneration age-chemical composition founded at higher metallicity ($Z \geq 0.01$). To solve this ambiguity *SBF color* versus *integrated color* diagrams are useful, since they appear to be strongly dependent on stellar populations properties (age and metallicity), and even more remarkably both quantities do *not* depend on distance determinations.

To quantify this theoretical expectation, in Fig. 17 we plot the selected theoretical SBF-color (involving $VIHK$ bands) versus the theoretical integrated color $(V-I)_0$. Theory predict up to 3.5 mag difference in $(\bar{M}_V - \bar{M}_K)$ for populations with extreme Z values, while nearly 3 mag in the $(\bar{M}_I - \bar{M}_K)$. Therefore, for stellar population analysis, it would be of the greatest interest to gain SBF measurements to built up the $(\bar{M}_V - \bar{M}_K)$ color.

In Figg. 18 and 19 observational data are compared to the theoretical SBF models in the $(\bar{M}_V - \bar{M}_I) - (V-I)_0$ and $(\bar{M}_I - \bar{M}_K) - (V-I)_0$ planes. In both figures the bulk of the galaxies is clearly concentrated near the position of the SSP having solar chemical composition and ages greater than 10 Gyr, i.e. the expected locus for early-type galaxies.

The models in the diagram of Fig. 18 are again sharply broken into two regions which identify different ranges in metallicity. This feature is substantiated by the location of the observational data: GGCs, which occupy the low-metallicity portion, and galaxies at redder $(V-I)_0$. As age increases, we expect a redder $(V-I)$ and bluer $(\bar{M}_V - \bar{M}_I)$, confirming results by BVA01.

As tracer of stellar population features, $(\bar{M}_V - \bar{M}_I)$ is not particularly accurate because of the superimposition of models with $0.01 \leq Z \leq 0.04$ clearly seen in Fig. 18. If one requires to disentangle the age-metallicity degeneracy, a better choice of SBF colors should be made. For example, $(\bar{M}_I - \bar{M}_K)$ and $(\bar{M}_V - \bar{M}_K)$ should be preferred. Concerning the $(\bar{M}_I - \bar{M}_K)$ color, Fig. 19 shows that the separation between models with different chemical composition is high enough to allow an evaluation of metallicity in spite of the non-negligible mean error of the observational SBF color. In particular, by adopting this kind of diagram the ambiguity shown in the K-band SBF (Fig. 16) for some galaxies can be solved. For instance, NGC 224 properties are now derived by simple interpolation of the SBF models. Similarly to NGC 224, we can take advantage by this diagram, and the age metallicity degeneration is fairly removed for several other galaxies. In Table 9 (columns 9–10) we summarize the results, reporting the age and metallicity values as inferred from

the location of the SBF measurements of each given galaxy in the $(\bar{M}_I - \bar{M}_K) - (V-I)_0$ plane.

One may note that the fair agreement found between the results in column (7–9) and (8–10) in Table 9 supports the general consistency of the two SBF methods. However, few galaxies show some differences. This is not surprising because several sources of uncertainty are at work, in a differential way, inside the two methods. Let us recall few of them: i) the distance moduli, ii) the presence of secondary populations, and iii) the reddening. Each of these requires evaluations or assumptions which affect the location of the observational points in the two diagrams.

Before concluding this Section, let us emphasize that all our results come from single-burst stellar population models. On this respect, we recall that by comparing their models with observations in the plane $(\bar{M}_I - \bar{M}_K)$ versus $(\bar{M}_V - \bar{M}_I)$, BVA01 conclude that composite stellar populations appear necessary for those galaxies with $(\bar{M}_V - \bar{M}_I) \leq 2.3$. On the other hand, the present models for simple stellar populations seem to match, at least within the observational uncertainties, the locus of the available measurements (see Fig. 20); in particular, the two Local Group galaxies NGC 221 and 224 are well fitted. Of course, in order to better reproduce the SBF of each individual galaxy (see for example the galaxy with the highest $\bar{M}_V - \bar{M}_I$: NGC 4472), it could be useful to introduce composite stellar populations, even if this implies to adopt *ad hoc scenarios* (see BVA01).

6. Useful relations

According with the above discussion, the single-burst models proposed in this work can be reliably adopted for both distance estimations and stellar population analysis. Some useful expressions can be given to obtain a straightforward determination of the SBF magnitudes once the integrated $(V-I)_0$ color of a galaxy has been measured. The least-squares method applied to theoretical models with ages $t \geq 9\ Gyr$ and metallicity $Z \geq 0.001$ (equivalently $(V-I)_0 \geq 0.95$) provides:

$$\bar{M}_V = (0.43 \pm 0.10) + (5.26 \pm 0.22)[(V-I)_0 - 1.15] \tag{2}$$

$$\bar{M}_R = (-0.52 \pm 0.14) + (5.37 \pm 0.31)[(V-I)_0 - 1.15] \tag{3}$$

$$\bar{M}_I = (-1.74 \pm 0.23) + (3.93 \pm 0.50)[(V-I)_0 - 1.15] \tag{4}$$

$$\bar{M}_K = (-5.22 \pm 0.23) - (3.87 \pm 0.50)[(V-I)_0 - 1.15]. \tag{5}$$

The relations presented here show a very good agreement for both V and I bands with the empirical calibrations by T01, and BVA01. The calibration of the R-band is fairly similar to the one presented by BVA01.

Concerning the $\bar{M}_K$ calibration, it appears quite different from the empirical result by LGC02. In particular, the theoretical calibration predicts an opposite trend with respect to the empirical one. This opposite behavior has been also discussed by LGC02; here we just point out that the age of the observed stellar population may play a relevant role. In fact Fig. 15(b) shows an age dependence of the K-band SBF amplitudes much larger than those expected in V and I bands (Fig. 15(a), and Fig. 14). More complex models (e.g LGC02), and further observations in the K-band are required to clarify this discrepancy. A similar result is obtained for $\bar{M}_{F160W}$ when the calibration is compared to the empirical one recently found by Jensen et al. (2003). Thus, the fact that NIR SBF age and metallicity variations have no degenerate effects, make quite problematic to derive accurate one-parameter SBF calibrations for these wavelengths.

In conclusion, the theoretical $\bar{M}_X$ versus $(V-I)_0$ relations agree well (but NIR filters) with the empirical relations, even in the simple adopted scenario of single-burst populations.

7. Conclusions

In this paper we have developed a new theoretical model for SBF predictions of simple stellar populations (single-burst, single chemical composition) with age ranging from 5 to 15 Gyr, and metallicity from 1/200 $Z_\odot$ to 2 $Z_\odot$, relatively to the standard $UBVRIJHK$ ground-based filters and the $F439W$, $F555W$, $F814W$, $F110W$, $F160W$, and $F222M$ of the HST photometric system (*WFPC2* and *NICMOS*). The model relies on the stellar population synthesis code developed by Brocato et al. (2000), optimized for a fine simulation of the latest (brightest) phases of stellar evolution, which has strong influence on SBF magnitudes.

The procedure adopted to compute the SBF amplitudes is different from previous theoretical works, and it has the advantage of being quite similar to the observational approach, currently used to measure the pixel to pixel fluctuation in real galaxies.

With this tool we simulated the effect of the mass loss processes along the RGB, the AGB and the TP. In particular, the impact of mass loss on the prediction of SBF magnitudes has been investigated, finding that a careful treatment of this quantity is fundamental in determining reliable SBF evaluations.

According to formalism by Reimers, we adopted $\eta_{RGB} = 0.4$ for the RGB stars. An independent calibration of the efficiency of mass loss along the AGB was performed by using the SBF technique. A set of models with different assumption on η_{AGB} was computed. The observed SBF measurements of GGCs and galaxies efficiently constraint the theoretical expectations, showing that the data are well reproduced by SSP of the proper age and metallicity if $\eta_{AGB} = 0.8$. Such value well agree with observational data (Le Bertre et al. 2001), and impressively reproduces the absolute K-band magnitude of the stars at the tip of the AGB in NGC 224. To our knowledge this is the first time that SBF measurements are used to constraints stellar evolution models of AGB stars.

We also compared our models with previous works (BVA01, LCG02), finding a substantial general agreement in spite of the different stellar evolution models adopted in the computations of the SSPs which generate the SBF evaluations.

The impact on SBF, due to the assumption on the IMF, is investigated and quantified by adopting a set of reasonable values of the exponent of a Scalo-like mass distribution. The consequences of cutting the IMF at a low mass limit are also presented. As expected, it is found that the contribution of upper part of the MS could not be neglected.

We investigate the effects on SBF predictions of different assumptions on the relation to transform theoretical quantities ($log\ L/L_{\odot}$ and $log\ T_{eff}$) to the observed magnitudes and colors. We find that the G87, CGK97, and LCB97 compilations provide quite similar SBF predictions for models with $Z < 0.01$, while sizeable differences should be expected if SSP of high Z are involved.

Once the theoretical framework defining the SSP models is fixed, we successfully checked the capability of deriving distances by our SBF predictions. This is done for a sample of GGCs for which SBF measurements are available and with a sample of properly selected galaxies of known distances.

As a result, a set of calibrations of absolute SBF magnitudes for classical $UBVRIJHK$ photometric bands and for selected HST filters is provided. The quoted test with other distance indicators (Cepheids, Planetary Nebula Luminosity Function, SBF empirical relations, etc.) shows that the degree of accuracy and precision of the present theoretical calibration of the absolute SBF magnitudes is sufficient to justify the use of these theoretical SBF as a *primary distance indicator*.

On the other side, we tested the use of SBF as tracers of stellar populations properties. In particular, we derived ages and metallicities for a subsample of galaxies for which SBF observations and reliable distances are available. The results appear very promising, since the obtained values are comparable with evaluation derived by other methods.

Moreover, *SBF color* versus *integrated color* diagrams are proposed as particularly useful in removing the well known age-metallicity degeneracy (e.g. Worthey 1994) which affects our knowledge of remote stellar systems.

Finally, we suggest that future observations should take advantage of the high sensibility of SBF measurements as stellar population tracers in the blue side of the spectral energy distribution of galaxies. This would be a meaningful scientific target for ground-based telescopes with high efficiency in the B wavelength range (VST) or for telescope located out of the earth atmosphere (HST, NGST).

Acknowledgments : Financial support for this work was provided by MIUR-Cofin 2000, under the scientific project "Stellar Observables of Cosmological Relevance". This project made use of computational resources granted by the Consorzio di Ricerca del Gran Sasso according to the Progetto 6 'Calcolo Evoluto e sue Applicazioni (RSV6)' - Cluster C11/B.

We thank the anonymous referee for a careful reading of the manuscript and for several useful suggestions for clarifying the presentation; his/her constructive report helped us to improve the paper.

A. APPENDIX: The Procedure

For sake of clearness we outline here the major steps of the procedure we have adopted to derive SBF magnitudes.

As a first step one needs to evaluate the total flux emitted by a stellar population generated by a single burst of star formation. In our model we make the assumption that the integrated light is dominated by the emission generated by stars of the simulated stellar system. This implies that i) no source of non-thermal emission are at work, ii) the thermal emission by interstellar gas gives no sizeable contribution to the integrated flux, and iii) the absorption from dust and gas are negligible. On this base, the integrated flux in a selected photometric filter (X) can be obtained by knowing two quantities:

$$f_X[L(m,t,Y,Z), T_{eff}(m,t,Y,Z), Y, Z], \tag{A1}$$

$$\Phi(m,N) \tag{A2}$$

where the f_X is the flux emitted by a star of mass m, age t (=stellar system age), luminosity L, effective temperature T_{eff}, and chemical composition (Y, Z). Obviously, f_X is defined by an extended library of homogeneous and self-consistent stellar evolutionary tracks (see Section 2), but it also depends on the adopted transformation tables (see par. 4.3).

The second quantity Φ is strictly related to the IMF and represents the number of stars with mass m in a population globally constituted of N stars with age t and chemical composition (Y, Z). A fundamental point is that the distribution of star masses along the IMF is obtained by using a Monte Carlo random method. A special attention was payed to ensure that, when a set of simulations with the same input parameters is computed, each distribution is fully independent from previous extractions.

Both the quantities are properly combined and integrated by the stellar population code to derive the total integrated flux F_X of the simulated stellar system in the selected photometric band:

$$F_X[N,t,Y,Z] = \sum_{i=1}^{N} f_X^i, \tag{A3}$$

thus this quantity evaluates absolute integrated flux of a stellar population of N stars with age t, chemical composition (Y, Z), and given IMF, as located at the reference distance of 10 pc.

If a number N^*_{sim} of simulations with exactly the same input parameters are computed, the resulting $F^j_X[N,t,Y,Z]$ is *not* expected to be constant since the initial mass distribution of each simulation is randomly generated. Thus, even if we adopt the same IMF law, each *j-th* mass distribution is fully independent from previous extractions. As a consequence, the resulting distribution of the stars in the CMD changes. In particular, the bright stars on the RGB/AGB (i.e. the most relevant contributors to the integrated light) are expected to undergo to sizeable variations in number and CMD position, and this qualitatively explains the fluctuations of F_X.

In principle, this can be considered quite similar to what happen in observing an ideal galaxy where the same population is spreaded in a number of pixels. Under the assumption of a ideal galaxy constituted of a homogeneous stellar population, the number and the luminosity of bright stars may change moving from pixel to pixel again due to Poisson statistical fluctuations. Thus, the measured flux in each pixel is expected to be affected by the fluctuations (TS88).

By following the formalism by Tonry and collaborators, we consider the amplitude of the expected fluctuations (SBF) $\bar{F}_X$ as the ratio of the variance to the average integrated flux, i.e.:

$$\bar{F}_X \equiv \frac{\langle F_X - \langle F_X \rangle \rangle^2}{\langle F_X \rangle} = \frac{\sum_j [F^j_X - \langle F_X \rangle]^2}{N^*_{sim} - 1} \cdot \frac{1}{\langle F_X \rangle}, \tag{A4}$$

where the average flux $\langle F_X \rangle$ of the selected population is given by:

$$\langle F_X \rangle = \frac{\sum_j F^j_X}{N^*_{sim}}. \tag{A5}$$

From the operational point of view, for each set of parameters (age, chemical composition, IMF, etc.) which identifies a stellar population model, we compute a large number of independent simulations ($N^*_{sim} = 5000$) deriving the F^j_X for each model. At this point the SBF flux is computed directly using the right terms of equation ($A4$) and the definition of ($A5$). Finally, the SBF flux is converted in the SBF magnitude $\bar{M}_X$ in usual way, being:

$$\bar{M}_X = -2.5 \; log \bar{F}_X. \tag{A6}$$

In order to compare our method for computing SBF with those obtained applying the "usual" procedure (i.e. to integrate the luminosity function times the squared flux per luminosity bin and divide by the total flux: TS88, BVA01, etc.), we directly computed, for several input parameters, the SBF values by using both our method and the usual one. To provide a quantitative example, we report in Table A1 the results for stellar population models with $t = 15\ Gyr$ and $Z = Z_\odot$.

The procedure outlined here gives SBF amplitudes in agreement with those obtained from the usual method, when the number of stars (N_{star}) in each simulation is so large that all the brightest bins in the luminosity function have a number of stars greater than zero. The condition

needed for a full equivalence of the two methods is satisfied when the limit of large numbers is approached (TS88). We find that this limit is reached when $N_{star} \gtrsim 10^8$ (in the mass interval $0.1 \leq \mathcal{M}/\mathcal{M}_{\odot} \leq 1.5$), just because the probability of finding very bright stars in each simulation becomes high enough. As N_{star} decreases, the differences between the SBF values computed by adopting the two methods increase.

Although the procedure outlined in this work is not particularly efficient in terms of computational time, it has some advantages. As a first point, the present approach to derive SBF amplitudes is more similar to the observational way of measuring SBFs in real galaxies. In fact, the opportunity of generating N_{sim} independent stellar populations each of them including N_{star} stars closely resembles what it is directly measured in N_{sim} pixels of a galaxy CCD image (neglecting the seeing effects), where the single pixel contains N_{star} stars. Here, we have typically adopted $N_{star} = 10^5$ which may represent the estimated number of stars per pixel for a galaxy in the Virgo cluster observed with a CCD having 0.3"/pix (Section 2). For such an assumption, the limit of large numbers is not satisfied. This implies a relatively small shift between the SBF amplitudes obtained with our procedure and the usual one as shown in Table A1 (Fig. 21).

As a new interesting results we suggest that the SBF magnitudes appear to have a small but not negligible dependence on the population (pixel) star density. Although this dependence is only a second order correction, it should be further investigated, both on theoretical and observational side, for a deeper understanding and a refining of the SBF method. In particular, we suggest that the present approach would be useful when dealing with SBF measurements obtained by pixels where the expected number of stars is relatively low (nearby galaxies, high resolution telescopes, loose galaxies) when compared with typical observations in ellipticals.

As a final consideration on the capability of the present way of computing SBF we note that it is also particularly efficient in handling the details of all the stellar evolutionary phases. In fact, each independent stellar population is computed by leaving to the statistics the possibility of distributing stars in the CMDs, according to their proper evolutionary pattern. On the other hand, the usual way makes use of predefinite isochrones which fix, by definition, one single pattern in the CMD (i.e. a fixed luminosity function) for each set of input parameters (t, Z). A relevant example is the HB stars distribution. As previously shown by Rood et al. (1973), the HB morphology can hardly be described by uniparametric (mass) curves as assumed when dealing with isochrones. In our procedure we always compute a synthetic HB which reproduces the color spread and relative star counts observed in real HBs (Brocato et al. 2000). Moreover, isochrones are generally computed by assuming a fixed value of mass loss rate along the RGB. On the contrary, in the present stellar population synthesis code the mass loss and its spread around an average value can be chosen as free input parameters (section 4.2.1).

REFERENCES

Ajhar, E.A., & Tonry, J.L. 1994, ApJ, 429, 557 (AT94)

Ajhar, E. A., Lauer, T. R., Tonry, J. L., Blakeslee, J. P., Dressler, A., Holtzman, J. A., & Postman, M. 1997, AJ, 114, 626

Alard, C. et al. 2001, ApJ, 552, 289

Alonso, A., Arribas, S., & Martinez-Roger, C. 1996, A&AS, 117, 227

Alonso, A., Arribas, S., & Martinez-Roger, C. 1999, A&AS, 140, 261

Baugh, C. M., Cole, S., Frenk, C. S., 1996, MNRAS, 283, 1361

Bell, R. A., 1973 MNRAS, 164, 197

Benedict, G., et al. 2002, AJ, 123, 473

Bertelli, G., Bressan, A., Chiosi, C., Fagotto, F., Nasi, E. 1994, A&AS, 106, 275

Bessel, M.S., 1979, PASP, 91, 589

Bica, E., Alloin, D., & Schmidt, A.A. 1990, A&A, 228, 23

Blakeslee, J.P., Vazdekis, A., & Ajhar, E.A. 2001, MNRAS, 320, 193 (BVA01)

Blakeslee, J.P., Ajhar, E.A., & Tonry J.L. 1999, in Astrophysics and space science library, 237, Post-Hipparcos cosmic candles, ed. A. Heck & F. Caputo (Boston : Kluwer Academic Publishers), 181

Blöcker, T., & Schönberner, D. 1997, A&A, 324, 991 (BS97)

Bono, G., Caputo, F., Cassisi, S., Castellani, V., & Marconi, M. 1997a, ApJ, 489, 822

Bono, G., Caputo, F., Cassisi, S., Castellani, V., & Marconi, M. 1997b, ApJ, 479, 279

Bressan, A., Chiosi, C., & Tantalo, R. 1996, A&A, 311, 425

Brocato, E., Capaccioli, M., & Condelli, M. 1998, Mem. SAIt, 69, 155

Brocato, E., Castellani, V., Poli, F.M., & Raimondo, G. 2000, A&AS, 146, 91 (BCPR00)

Brocato, E., Castellani, V., Raimondo, & G., Romaniello M. 1999, A&AS, 136, 65

Brocato, E., Matteucci, F., Mazzitelli, I., & Tornambè, A. 1990, ApJ, 349, 458

Busarello, G., Capaccioli, M., D'Onofrio, M., Longo, G., Richter, G., & Zaggia, S. 1996, A&A, 314, 32

Buzzoni, A. 1993, A&A, 275, 433 (B93)

Cantiello, M. 2001, Physics Diploma Thesis, Univ. di Napoli

Carollo, C.M., Danziger, I.J., & Buson, L. 1993, MNRAS, 265, 553

Cassisi, S., Castellani, V., degl'Innocenti, S., & Weiss, A. 1998 A&AS, 129, 267

Castellani, V., Chieffi, A., & Pulone, L. 1991, ApJS, 76, 911

Castellani V., Chieffi S., & Straniero O. 1992, ApJS 78, 517

Castellani, V., & Tornambè, A. 1991, ApJ, 381, 339

Castelli, F., Gratton, R.G., & Kurucz, R.L. 1997, A&A, 318, 841 (CGK97)

Ciardullo, R., Feldmeier, J.J., Jacoby G.H., Kuzio de Naray, R. , Laychak M.B., & Durrell, P.R. 2002, ApJ, 577, 31

Cousins, A.W.J. 1976, MmRAS, 81, 25

Cousins, A.W.J. 1978, MNSSA, 37, 82

Davidge, T.J. 1997, AJ, 113, 985

Davidge, T.J. 2001, AJ, 122, 1386

Ferrarese, L., et al. 2000, ApJS, 128, 431

Ferreras, I., Charlot, S., & Silk, J. 1999, ApJ, 521, 81

Freedman, W. L., et al. 2001, ApJ, 553, 47

Freeman, K. C., & Norris J. 1981, ARA&A, 19, 319

Girardi, L., Bressan, A., Bertelli, G., Chiosi, C. 2000 A&AS, 141, 137

Green, E.M., Demarque, P., & King, C.R. 1987, in The revised Yale isochrones and luminosity functions, New Haven: Yale Observatory (G87)

Greggio, L., & Renzini, A. 1990, ApJ, 364, 35

Groenewegen M.A.T., & de Jong, T. 1993, A&A, 267, 401

Harris, W. 1999, http://physun.physics.mcmaster.ca/Globular.html

Henry, R.B.C., & Worthey, G. 1999, PASP, 111, 919

Jacoby, G. H., et al. 1992, PASP, 104, 599

Jensen, J.B., Luppino, G.A., & Tonry, J.L. 1996, ApJ, 468, 519

Jensen J.B., Tonry, J.L., Barris, B.J., Thompson, R.I., Liu, M.C., Rieke, M.J., Ajhar, E.A., Blakeslee, J.P., 2003, ApJ, 583, 712

Jensen, J.B., Tonry, J.L., & Luppino, G.A. 1998, ApJ, 510, 71

Jensen, J. B., Tonry, J. L., Thompson, R. I., Ajhar, E. A., Lauer, T. R., Rieke, M. J., Postman, M., & Liu, M. C. 2001, ApJ, 550, 503

Jerjen, H., Binggeli, B., & Freeman, K. C. 2000, AJ, 119, 593

Jerjen, H., Freeman, K. C., & Binggeli, B. 1998, AJ, 116, 2873

Jerjen, H., Rekola, R., Takalo, L., Coleman, M., & Valtonen, M. 2001, A&A, 380, 9

Johnson, H.L., & Morgan, W.W. 1953, ApJ, 117, 313

Kauffmann, G., & Charlot S. 1998, MNRAS, 294, 705

Kobayashi, C., & Arimoto, N. 1999, ApJ, 527, 573

Kudriztki, R.P., Pauldrach, A., & Puls, J. 1987, A& A, 173, 293

Kurucz, R.L. 1979, ApJS, 40, 1

Le Bertre, T., Matsuura, M., Winters, J.M., Murakami, H., Yamamura, I., Freund, M., & Tanaka, M. 2001, A&A, 376, 997

Lee, Y.-W., Demarque, P., & Zinn, R., 1987, in Conference on Faint Blue Stars, Schenectady, NY, L. Davis Press, Inc., 137

Lejeune, T., Cuisinier, F., & Buser, R. 1997, A&AS, 125, 229 (LCB97)

Liu, M.C., Graham, J.R., & Charlot S. 2002, ApJ, 564, 216 (LGC02)

Liu, M.C., Charlot, S., & Graham, J.R. 2000, ApJ, 543, 644 (LCG00)

Lorenz, H., Böhm, P., Capaccioli, M., Richter, G.M., & Longo, G. 1993, A&A, 277, 15

Luppino, G.A., & Tonry, J.L. 1993, ApJ, 410, 81

Mei, S., Quinn, P.J., & Silva, D.R. 2001, A&A, 317, 779

Mould, J.R. 2000, ApJ, 529, 786

Neilsen, E.H., & Tsvetanov, Z.I. 2000, 536, 255

Origlia, L., & Leitherer, C. 2000, AJ, 119, 2018 (OL00)

Pahre, M. A. 1999, ApJ, 515, 79

Pahre, M.A., & Mould, J.R. 1994, ApJ, 433, 567

Peletier, R.F., Davies, R.L., Illingworth, G.D., Davis, L.E., Cawson, M. 1990, AJ, 100, 1091

Reid, I. N. 1998, in ASP Conference Series, 142, The stellar initial mass function (38th Herstmonceux Conference), ed. G. Gilmore & D. Howell, 121

Reimers, D. 1975, in Problems in stellar atmospheres and envelopes, (New York: Springer-Verlag), 229

Renzini, A. 1981, in Proceedings of the Fifty-ninth Colloquium, Trieste, Italy, Effects of mass loss on stellar evolution (Dordrecht, D. Reidel Publishing Co.), 319

Renzini, A. 1998, AJ, 115, 2459

Renzini, A., & Buzzoni, A. 1986, in Proceedings of the Fourth Workshop, Erice, Italy, March 12-22, 1985, Spectral evolution of galaxies (Dordrecht, D. Reidel Publishing Co.),195

Renzini, A., & Fusi Pecci, F. 1988, ARA&A 26, 199

Rood, R. T. 1973, ApJ, 184, 815

Saglia, R.P., Maraston, C., Thomas, D., Bender, R., & Colless M. 2002, ApJ, 579, L13

Salpeter, E.E. 1955, ApJ, 121, 161

Scalo, J.M. 1986, Fundamental of Cosmic Physics, 11, 1

Sodemann, M., & Thomsen, B. 1995, AJ, 110, 179

Terlevich, A.I., & Forbes, D.A. 2002, MNRAS, 330, 547 (TF02)

Tonry, J.L., Dressler, A., Blakeslee, J.P., Ajhar, E. A., Fletcher, A. B., Luppino, G.A., Metzger, M.R., & Moore, C. B. 2001, ApJ, 546, 681 (T01)

Tonry, J.L., Blakeslee, J.P, Ajhar, E.A., & Dressler, A. 1997, ApJ, 475, 399 (TBAD97)

Tonry, J.L., Ajhar, E.A., & Luppino G.A. 1990, AJ, 100, 1416 (TAL90)

Tonry, J.L., & Schechter P.L. 1990, AJ, 100, 1794

Tonry, J.L., & Schneider D.P. 1988, AJ, 96, 807 (TS88)

Trager, S.C., Faber, S.M., Worthey, G., & Gonzalez, J.J. 2000, AJ, 120, 165 (TFWG00)

Vassiliadis, E., & Wood, P.R. 1994, ApJS, 92, 125 (VW94)

Weiss, A., Peletier, R.F., & Matteucci, F. 1995, A&A, 296, 73

Worthey, G. 1993, ApJ, 415, 91 (W93)

Worthey, G. 1994, ApJS, 95, 107

This preprint was prepared with the AAS LaTeX macros v5.0.

Fig. 1.— Simulated Color-Magnitude Diagrams for a fixed age (t=15 Gyr) and for three values of metallicity: Z=0.001 (triangles), 0.01 (stars), 0.02 (circles). A solar metallicity population with $t = 15$ Gyr, transformation tables are from Castelli, Gratton & Kurucz (1997).

Fig. 2.— SBF amplitude $\bar{M}_I$ as a function of the number of Monte Carlo cycles. For N_{sim} >1000, $\bar{M}_I$ varies around the asymptotic value (the permitted region is delimited by the dashed lines) by an amount well within the typical observational uncertainties (∼0.05). The arrow indicates the value N^*_{sim}=5000 adopted in our calculations (see text).

Fig. 3.— *(a)* Predicted SBF absolute magnitudes within $UBVRIJHK$ ground-based filters for reference models aged 15 Gyr (solid line) and 5 Gyr (dashed line) versus the metal content. LCB97 transformations were adopted. The selected passbands are marked with different symbols, as labeled.
(b) **As in panel** *(a)* **but for HST filters. In this case we adopt OL00 transformations.**

Fig. 4.— Predicted SBF absolute magnitudes within $UBVRIJHK$ filters for reference models versus the age of the stellar population ($Z = 0.02$ solid lines, $Z = 0.0001$ dashed lines). The selected passbands are marked with different symbols, as labeled.

Fig. 5.— Comparison between SBF synthetic models with similar age: LGC02 models with $t = 17$ Gyr (dotted line and four pointed stars); BVA01 models $t = 15.8$ Gyr (dashed line and three pointed stars); present work models with $t = 15$ Gyr (solid line and filled circles).

Fig. 6.— The effect of the mass loss variations along the RGB on $UVIK$ bands SBF magnitudes. The mass loss is parameterized by the η coefficient of the Reimers formula. The dotted line refers to $Z = 0.04$, the solid line to $Z = 0.02$, and the dashed line to $Z = 0.01$. All models refer to $t = 15$ Gyr populations. For graphical reasons we shifted all non solar models to match the SBF values of the solar model with η=0.2.

Fig. 7.— The behavior of SBF magnitudes in the $IJHK$ bands as function of the $(V-I)_0$ integrated color. A stellar population of solar chemical composition is assumed. The size of the symbols marks increasing values of η_{AGB} (0.4, 0.8, 1.6, and 3.2); see also the orientation of the labeled arrow. The other arrow indicates the orientation of increasing ages (5, 9, 11, 13, 15 Gyr) that are also linked by dotted lines.

Fig. 8.— Theoretical models (open symbols) obtained by adopting the labeled values of η_{AGB} are compared with the empirical calibration by T01 (slanted solid line). The horizontal solid line refers to the observational locus of GGCs. Each symbol indicates a different chemical composition: $Z = 0.0001$ (three-pointed stars); $Z = 0.001$ (four-pointed stars); $Z = 0.01$ (five-pointed stars); $Z = 0.02$ (triangles); $Z = 0.04$ (squares). The symbol size increases according to age (t = 5, 9, 11, 13, and 15 Gyr). The arrows indicate the directions of the evolution with age and metallicity. Both the horizontal and the slanted lines suffer of an uncertainty in the zero point as large as 0.15 and 0.20 mag, respectively (shadowed regions).

Fig. 9.— $UBVI$ bands SBF magnitudes versus the number density of PAGB stars relative to HB stars (N_{PAGB}/N_{HB}). Solid lines refer to the BS97 and dashed lines to VW94 PAGB models. The shadowed region indicates the proper ratio predicted for our reference models. A solar metallicity population ($Z = 0.02$) with age $t = 15$ Gyr is assumed.

Fig. 10.— The effects of transformations tables on SBF amplitudes are illustrated as a function of metallicity. The residuals are computed as: $\Delta\bar{M} = SBF_X - SBF_{LCB97}$, where $X = CGK97$ (dotted line, filled triangles) or $X = G87$ (long-dashed line, open squares). An age of $t = 15$ Gyr is considered.

Fig. 11.— The solar metallicity isochrone (t=15 Gyr) is transformed with LCB97 (bold solid line), CGK97 (dotted line), G87 (dashed line), and Alonso et al. 1996-1999 (long-dashed line). The three panels show respectively: V versus $(V-I)_0$, I versus $(V-I)_0$, and K versus $(V-I)_0$. V, I, and K are the absolute magnitudes. The star indicates where the extrapolation on colors for CGK97 tables ($T_{eff} < 3500$ K) begins. Alonso et al. (1999) models have nearly the same limit, being the minimum temperature tabulated $T_{min} = 3750$ K.

Fig. 12.— Our SBF predictions (open triangles) in V and I bands plotted against the observational data of 19 GGCs (AT94, open circles). Models of increasing age are marked with larger symbols (t = 5, 9, 11, 13, 15 Gyr); the solid (long-dashed) line connects models with $t = 15$ Gyr ($t = 5$ Gyr) for different chemical compositions. Dotted lines represent the best-fit as derived by BVA01 (see text).

Fig. 13.— Theoretical I-band SBF are compared to observed data. $\bar{M}_I$ for observed galaxies is derived by adopting the distance modulus from the Period-Luminosity relation of Cepheids variables (Ferrarese et al. 2000). Symbols are as in Fig. 8.

Fig. 14.— As in Fig. 13, but for a sample of galaxies with distances measured from other distance indicators. Distance moduli are again from Ferrarese et al. (2000).

Fig. 15.— *(a)* As in Fig. 14, but for $\bar{M}_V$. Galaxies with Cepheids-based distances are added (circled dots).

Fig. 15.— *(b)* As in *(a)*, but for $\bar{M}_K$. Filled circles are K' measurements, while open circles K_s. Galaxies with multiple observations are still plotted using different symbols.

Fig. 15.— *(c)* As in *(a)*, but for $\bar{M}_{F160W}$. We note that NGC 4278 has distance measurements with a large spread, if compared to internal uncertainties (Ferrarese et al. 2000).

Fig. 16.— The subsample of galaxies with age and metallicity estimations from the literature are plotted against theoretical models for all ages and metallicity higher than half-solar. The galaxies are identified at the top of each panel according to the increasing integrated $(V-I)_0$ color. For each galaxy we also report the size of the depth of its group according to Ferrarese et al. (2000).

Fig. 17.— Theoretical *SBF color* versus *integrated* $(V-I)_0$ *color* diagrams obtained with our fluctuations models. Note the major excursion of the $(\bar{M}_V - \bar{M}_K)$ color for extreme Z values, compared to other SBF colors. Symbols are as in Fig. 8.

Fig. 18.— The $(\bar{M}_V - \bar{M}_I)$ color is plotted against the integrated color $(V-I)_0$. Open circles refer to GGCs data, and filled circles to galaxies. The typical error bars of GGCs data are also plotted.

Fig. 19.— The $(\bar{M}_I - \bar{M}_K)$ color is plotted against the integrated color $(V-I)_0$. For clarity we only plot models with the highest metallicity considered.

Fig. 20.— The $(\bar{M}_V - \bar{M}_I)$ versus the $(\bar{M}_I - \bar{M}_K)$ color are plotted for the new models (symbols as in Fig. 8) and observational data. The observed SBF amplitudes of galaxies are: V-band from BVA01 (filled circles), TAL90 (open circles), and AT94 (NGC 224); I-band from T01; K-band from Luppino & Tonry (1993) and Jensen et al. (1998).

Fig. 21.— SBF amplitudes obtained with the "usual" (dashed line) and the "present work" (filled circles) procedures versus N_{star}.

Table 1a. Surface Brightness Fluctuations for the reference models: ground-based filters

Z	Y	Age	$\bar{M}_U$	$\bar{M}_B$	$\bar{M}_V$	$\bar{M}_R$	$\bar{M}_I$	$\bar{M}_J$	$\bar{M}_H$	$\bar{M}_K$	$(V-I)$
0.0001	0.23	5	1.711	0.934	-0.776	-1.771	-2.690	-3.719	-4.456	-4.658	0.776
		9	1.527	0.759	-0.815	-1.738	-2.592	-3.564	-4.266	-4.457	0.855
		11	1.552	0.774	-0.719	-1.596	-2.409	-3.355	-4.035	-4.218	0.858
		13	1.577	0.827	-0.636	-1.490	-2.283	-3.216	-3.884	-4.062	0.871
		15	1.534	0.811	-0.610	-1.425	-2.185	-3.102	-3.752	-3.923	0.891
0.001	0.23	5	2.426	1.176	-0.685	-1.776	-2.817	-4.009	-4.949	-5.184	0.913
		9	2.304	1.131	-0.571	-1.548	-2.464	-3.564	-4.441	-4.650	0.965
		11	2.367	1.198	-0.474	-1.424	-2.306	-3.375	-4.235	-4.434	0.977
		13	2.183	1.141	-0.478	-1.404	-2.260	-3.312	-4.158	-4.349	0.980
		15	2.008	1.080	-0.425	-1.331	-2.174	-3.215	-4.057	-4.244	0.959
0.01	0.255	5	3.476	1.801	0.055	-1.037	-2.495	-4.348	-5.488	-5.839	1.075
		9	3.386	1.875	0.237	-0.797	-2.164	-4.027	-5.153	-5.542	1.114
		11	3.388	1.887	0.256	-0.775	-2.126	-3.868	-4.982	-5.339	1.130
		13	3.351	1.902	0.283	-0.758	-2.104	-3.728	-4.816	-5.152	1.151
		15	3.324	1.927	0.332	-0.697	-2.011	-3.644	-4.732	-5.082	1.167
0.02	0.289	5	4.124	2.247	0.528	-0.489	-1.918	-4.518	-5.656	-6.145	1.112
		9	4.230	2.352	0.702	-0.270	-1.671	-4.064	-5.190	-5.633	1.174
		11	4.169	2.325	0.710	-0.238	-1.612	-4.025	-5.150	-5.600	1.196
		13	4.111	2.344	0.759	-0.173	-1.526	-3.883	-5.010	-5.447	1.211
		15	4.085	2.353	0.781	-0.152	-1.513	-3.846	-4.974	-5.402	1.229
0.04	0.34	5	4.796	2.715	0.987	0.013	-1.411	-4.554	-5.654	-6.203	1.188
		9	4.792	2.763	1.116	0.193	-1.121	-4.120	-5.241	-5.770	1.249
		11	4.797	2.769	1.140	0.230	-1.045	-3.984	-5.111	-5.630	1.271
		13	4.779	2.804	1.198	0.299	-0.980	-3.948	-5.083	-5.600	1.288
		15	4.740	2.786	1.198	0.306	-0.960	-3.882	-5.012	-5.522	1.304

Table 1b. Surface Brightness Fluctuations for the reference models: HST filters

Z	Y	Age	$\bar{M}_{F439W}$	$\bar{M}_{F555W}$	$\bar{M}_{F814W}$	$\bar{M}_{F110W}$	$\bar{M}_{F160W}$	$\bar{M}_{F222M}$	$(V-I)$
0.0001	0.23	5	1.141	-0.794	-2.752	-3.442	-4.414	-4.566	0.776
		9	0.936	-0.834	-2.654	-3.302	-4.228	-4.370	0.855
		11	0.933	-0.735	-2.471	-3.099	-3.999	-4.133	0.858
		13	0.981	-0.650	-2.345	-2.963	-3.849	-3.978	0.871
		15	0.965	-0.623	-2.247	-2.853	-3.720	-3.842	0.891
0.001	0.23	5	1.410	-0.696	-2.897	-3.720	-4.873	-5.088	0.913
		9	1.339	-0.580	-2.541	-3.287	-4.374	-4.560	0.965
		11	1.402	-0.482	-2.382	-3.103	-4.170	-4.346	0.977
		13	1.331	-0.486	-2.336	-3.041	-4.095	-4.263	0.980
		15	1.233	-0.433	-2.249	-2.946	-3.995	-4.159	0.959
0.01	0.255	5	2.095	0.103	-2.625	-4.073	-5.394	-5.788	1.075
		9	2.117	0.240	-2.329	-3.738	-5.055	-5.455	1.114
		11	2.136	0.272	-2.272	-3.596	-4.882	-5.252	1.130
		13	2.161	0.327	-2.192	-3.472	-4.747	-5.097	1.151
		15	2.176	0.366	-2.120	-3.381	-4.644	-4.994	1.167
0.02	0.289	5	2.466	0.496	-2.246	-4.583	-5.605	-6.024	1.112
		9	2.567	0.675	-1.937	-3.737	-5.120	-5.515	1.174
		11	2.534	0.682	-1.890	-3.700	-5.081	-5.478	1.196
		13	2.547	0.733	-1.789	-3.564	-4.936	-5.327	1.211
		15	2.555	0.753	-1.770	-3.531	-4.897	-5.285	1.229
0.04	0.34	5	2.890	0.944	-1.791	-4.202	-5.741	-6.251	1.188
		9	2.930	1.077	-1.516	-3.779	-5.272	-5.756	1.249
		11	2.935	1.104	-1.437	-3.647	-5.120	-5.591	1.271
		13	2.967	1.163	-1.395	-3.613	-5.079	-5.545	1.288
		15	2.947	1.163	-1.368	-3.550	-5.005	-5.465	1.304

Table 2. SBF amplitudes for different assumptions on the lowest mass limit ($\mathcal{M}_{low}$) for a population model with $t = 15\ Gyr$, $Z = 0.02$, $Y = 0.289$

$\mathcal{M}_{low}$	$\bar{M}_U$	$\bar{M}_B$	$\bar{M}_V$	$\bar{M}_R$	$\bar{M}_I$	$\bar{M}_J$	$\bar{M}_H$	$\bar{M}_K$
0.85	3.886	2.146	0.571	-0.374	-1.716	-3.914	-5.024	-5.425
0.60	4.106	2.361	0.775	-0.174	-1.534	-3.769	-4.896	-5.306
0.40	4.117	2.377	0.798	-0.142	-1.487	-3.717	-4.845	-5.255
0.10	4.112	2.385	0.811	-0.122	-1.451	-3.668	-4.798	-5.205

Table 3. SBF amplitudes for different IMF slopes x (see text) for a population model with $t = 15\ Gyr$, $Z = 0.02$, $Y = 0.289$

x	$\bar{M}_U$	$\bar{M}_B$	$\bar{M}_V$	$\bar{M}_R$	$\bar{M}_I$	$\bar{M}_J$	$\bar{M}_H$	$\bar{M}_K$
0.35	4.029	2.300	0.733	-0.198	-1.552	-3.889	-5.011	-5.441
1.35	4.085	2.353	0.781	-0.153	-1.513	-3.846	-4.974	-5.402
2.35	4.170	2.441	0.873	-0.049	-1.385	-3.703	-4.838	-5.263

Table 4. SBF amplitudes for simple stellar populations with age $t = 15\ Gyr$ and different values of Reimers' coefficient η

Z	η	$\bar{M}_U$	$\bar{M}_B$	$\bar{M}_V$	$\bar{M}_R$	$\bar{M}_I$	$\bar{M}_J$	$\bar{M}_H$	$\bar{M}_K$	$(V-I)$
0.01	0.2	3.342	1.915	0.329	-0.682	-2.054	-3.853	-4.976	-5.341	1.173
	0.4	3.324	1.927	0.332	-0.697	-2.011	-3.644	-4.732	-5.082	1.167
	0.6	3.009	1.885	0.367	-0.623	-1.890	-3.542	-4.634	-4.990	1.148
	0.8	2.284	1.620	0.417	-0.540	-1.850	-3.563	-4.673	-5.036	1.078
0.02	0.2	4.092	2.345	0.774	-0.159	-1.552	-4.035	-5.163	-5.618	1.234
	0.4	4.085	2.353	0.781	-0.152	-1.513	-3.846	-4.974	-5.402	1.229
	0.6	4.023	2.375	0.818	-0.116	-1.459	-3.699	-4.827	-5.237	1.221
	0.8	3.578	2.273	0.791	-0.122	-1.418	-3.621	-4.756	-5.164	1.201
0.04	0.2	4.746	2.780	1.186	0.288	-1.004	-4.062	-5.192	-5.719	1.311
	0.4	4.740	2.786	1.198	0.306	-0.960	-3.882	-5.012	-5.522	1.304
	0.6	4.646	2.758	1.188	0.305	-0.945	-3.761	-4.889	-5.388	1.292
	0.8	4.186	2.638	1.160	0.307	-0.898	-3.696	-4.835	-5.338	1.260

Table 5. SBF amplitudes for simple stellar populations with $Z = 0.02$, $Y = 0.289$, and different assumptions for η_{AGB}

η_{AGB}	*Age*	$\bar{M}_U$	$\bar{M}_B$	$\bar{M}_V$	$\bar{M}_R$	$\bar{M}_I$	$\bar{M}_J$	$\bar{M}_H$	$\bar{M}_K$	$(V-I)$
0.4	5	4.122	2.245	0.526	-0.499	-2.047	-5.145	-6.275	-6.803	1.137
	9	4.226	2.350	0.700	-0.279	-1.778	-4.607	-5.731	-6.235	1.192
	11	4.168	2.325	0.711	-0.241	-1.684	-4.448	-5.575	-6.075	1.208
	13	4.111	2.344	0.760	-0.175	-1.598	-4.325	-5.455	-5.950	1.222
	15	4.084	2.353	0.782	-0.153	-1.550	-4.106	-5.236	-5.704	1.237
0.8	5	4.124	2.247	0.528	-0.489	-1.918	-4.518	-5.656	-6.145	1.112
	9	4.230	2.352	0.702	-0.270	-1.671	-4.064	-5.190	-5.633	1.174
	11	4.169	2.325	0.710	-0.238	-1.612	-4.025	-5.150	-5.600	1.196
	13	4.111	2.344	0.759	-0.173	-1.526	-3.883	-5.010	-5.447	1.211
	15	4.085	2.353	0.781	-0.152	-1.513	-3.846	-4.974	-5.402	1.229
1.6	5	4.127	2.249	0.530	-0.482	-1.849	-4.129	-5.257	-5.697	1.102
	9	4.232	2.353	0.702	-0.268	-1.627	-3.826	-4.949	-5.356	1.166
	11	4.173	2.327	0.712	-0.234	-1.567	-3.745	-4.867	-5.268	1.188
	13	4.116	2.346	0.760	-0.170	-1.485	-3.660	-4.783	-5.184	1.204
	15	4.088	2.354	0.781	-0.150	-1.474	-3.670	-4.795	-5.194	1.222
3.2	5	4.130	2.251	0.531	-0.478	-1.794	-3.742	-4.849	-5.204	1.093
	9	4.233	2.352	0.699	-0.269	-1.584	-3.614	-4.731	-5.102	1.158
	11	4.177	2.330	0.714	-0.226	-1.567	-3.583	-4.703	-5.089	1.178
	13	4.121	2.352	0.770	-0.150	-1.415	-3.552	-4.681	-5.082	1.193
	15	4.099	2.377	0.819	-0.093	-1.383	-3.606	-4.741	-5.154	1.208

Table 6. SBF amplitudes for different color-temperature relations (see text). An age $t = 15\ Gyr$ is assumed

Z	$\bar{M}_U$	$\bar{M}_B$	$\bar{M}_V$	$\bar{M}_R$	$\bar{M}_I$	$\bar{M}_J$	$\bar{M}_H$	$\bar{M}_K$
LCB97 Atmospheres transformations								
0.0001	1.533	0.811	-0.610	-1.424	-2.184	-3.101	-3.751	-3.923
0.001	2.008	1.080	-0.424	-1.330	-2.173	-3.215	-4.056	-4.244
0.01	3.324	1.926	0.331	-1.697	-2.011	-3.644	-4.732	-5.081
0.02	4.085	2.352	0.781	-1.152	-1.512	-3.846	-4.973	-5.402
0.04	4.740	2.786	1.198	0.305	-0.960	-3.881	-5.012	-5.521
CGK97 Atmospheres transformations								
0.0001	1.579	0.817	-0.522	-1.271	-2.004	-3.142	-3.869	-4.048
0.001	2.108	1.072	-0.427	-1.259	-2.050	-3.281	-4.161	-4.368
0.01	3.433	1.863	0.128	-0.850	-1.933	-3.661	-4.830	-5.145
0.02	4.094	2.253	0.496	-0.510	-1.474	-3.815	-5.094	-5.416
0.04	4.844	2.660	0.878	-0.125	-1.121	-3.803	-5.218	-5.585
G87 Atmospheres transformations								
0.0001	1.587	0.828	-0.432	-1.248	-1.943	···	···	···
0.001	2.067	1.037	-0.426	-1.274	-2.044	···	···	···
0.01	3.013	1.769	0.151	-0.850	-2.087	···	···	···
0.02	3.355	2.049	0.515	-0.468	-2.033	···	···	···
0.04	3.743	2.338	0.863	-0.075	-2.084	···	···	···

Table 7. Measured SBF amplitudes $\bar{m}_V$ and $\bar{m}_I$, and $(V-I)_0$ color are from AT94. Other GGCs properties are from Harris (1999)

GGC Name	$\bar{m}_V$	$\bar{m}_I$	E_{B-V}	$(V-I)_0$	M_V^{tot}	$[Fe/H]$	DM
NGC 104 (47Tuc)	13.15 ± 0.08	11.10 ± 0.16	0.04	1.06	−9.42	−0.76	13.37
NGC 288	14.53 ± 0.34	12.57 ± 0.45	0.03	0.92	−6.60	−1.24	14.69
NGC 2419	19.29 ± 0.09	17.72 ± 0.12	0.11	0.85	−9.58	−2.34	19.97
NGC 5139	13.67 ± 0.10	12.01 ± 0.12	0.12	0.95	−10.29	−1.62	13.97
NGC 5272 (M3)	14.37 ± 0.14	12.59 ± 0.17	0.01	0.88	−8.93	−1.57	15.12
NGC 5904 (M5)	14.04 ± 0.16	12.30 ± 0.19	0.03	0.89	−8.81	−1.29	14.46
NGC 6093 (M80)	14.84 ± 0.18	12.90 ± 0.21	0.18	0.99	−8.23	−1.75	15.56
NGC 6205 (M13)	13.68 ± 0.16	12.05 ± 0.20	0.02	0.88	−8.70	−1.54	14.48
NGC 6341 (M92)	13.85 ± 0.17	12.23 ± 0.20	0.02	0.86	−8.20	−2.29	14.64
NGC 6624	15.45 ± 0.20	12.40 ± 0.27	0.28	1.20	−7.50	−0.42	15.37
NGC 6626 (M28)	14.41 ± 0.18	11.86 ± 0.22	0.43	1.01	−8.33	−1.45	15.12
NGC 6637 (M69)	15.30 ± 0.11	12.91 ± 0.19	0.16	1.07	−7.52	−0.71	15.16
NGC 6652	15.43 ± 0.13	13.48 ± 0.22	0.09	1.03	−7.73	−0.96	15.19
NGC 6656 (M22)	12.96 ± 0.21	10.83 ± 0.26	0.34	1.00	−8.50	−1.64	13.60
NGC 6715 (M54)	16.93 ± 0.12	15.16 ± 0.13	0.14	0.90	−10.01	−1.59	17.61
NGC 6723	14.88 ± 0.13	13.23 ± 0.22	0.05	1.01	−7.86	−1.12	14.87
NGC 7006	17.53 ± 0.18	16.03 ± 0.21	0.05	0.92	−7.68	−1.63	18.24
NGC 7078 (M15)	14.65 ± 0.11	13.06 ± 0.13	0.10	0.83	−9.17	−2.25	15.37
NGC 7089 (M2)	14.89 ± 0.09	13.29 ± 0.11	0.06	0.91	−9.02	−1.62	15.49

Table 8. The selected galaxy sample

alaxy	T[a]	A_B[a]	$(V-I)_0$[a]	$\bar{m}_I$[a]	$\bar{m}_V$	Ref.	$\bar{m}_R$	Ref.	$\bar{m}_{K'}$	Ref.	$\bar{m}_{Ks}$	Ref.	$\bar{m}_{F814W}$	Ref.	$\bar{m}_{F160W}$	Ref.	DM
pheids distance determination																	
0224	3	0.35	1.231±0.007	23.03±0.05	25.29±0.08	1	···		18.80±0.21	5	18.82±0.09	8	23.54±0.04	11	19.78±0.04	12	24.44±0.10
3031	2	0.35	1.187±0.011	26.38±0.25	29.07±0.27	1	···		···		···		···		22.99±0.05	12	27.80±0.08
3351		0.12	1.225±0.014	···	···		···		···		···		···		25.19±0.07	12	30.01±0.08
3368	2	0.11	1.145±0.015	28.32±0.20	···		···		···		···		···		24.88±0.09	12	30.20±0.10
4258	4	0.07	1.134±0.023	27.50±0.08	···		···		···		···		···		···		29.49±0.07[b]
4548	3	0.16	1.148±0.019	29.67±0.53	···		···		···		···		···		···		31.04±0.08
4725	2	0.05	1.209±0.023	29.14±0.32	···		···		···		···		···		25.72±0.10	12	30.57±0.08
7331	3	0.39	1.120±0.017	28.72±0.14	···		···		···		···		···		25.43±0.08	12	30.89±0.10
her distance determination																	
0221	-6	0.35	1.133±0.007	22.73±0.05	25.14±0.10	2	24.36±0.10	2	18.56±0.09	6	18.56±0.08	8	22.84±0.03	11	19.11±0.05	12	24.56±0.17
0891	3	0.28	1.142±0.017	27.83±0.11	···		···		···		···		···		···		29.95±0.05
1023	-3	0.26	1.193±0.017	28.74±0.13	···		···		···		···		29.11±0.04	11	···		30.23±0.08
1316	-2	0.09	1.132±0.016	29.83±0.15	32.25±0.16	3	···		···		···		···		26.11±0.09	12	31.28±0.09
1399	-5	0.06	1.227±0.016	30.11±0.13	32.47±0.12	3	···		25.98±0.16	7	26.14±0.12	10	···		26.79±0.04	12	31.31±0.09
1404	-5	0.05	1.224±0.016	30.20±0.16	32.48±0.12	3	···		25.82±0.14	7	25.89±0.05	10	···		26.69±0.08	12	31.33±0.10
3115	-3	0.20	1.183±0.010	28.34±0.06	···		···		···		···		···		···		30.05±0.10
3377	-5	0.15	1.114±0.009	28.35±0.06	30.57±0.11	1	···		···		···		28.59±0.05	11	···		30.19±0.08
3379	-5	0.10	1.193±0.015	28.57±0.07	31.21±0.06	2	30.36±0.05	2	···		24.72±0.06	9	28.81±0.11	13	25.26±0.08	12	30.23±0.06
3384	-3	0.11	1.151±0.018	28.59±0.10	···		···		···		···		28.87±0.02	11	25.34±0.17	12	30.28±0.08
4278	-5	0.12	1.161±0.012	29.34±0.18	···		···		···		···		···		26.38±0.09	12	30.51±0.14
4374	-5	0.17	1.191±0.008	29.77±0.09	32.02±0.09	2	31.22±0.07	2	···		25.43±0.22	8	30.02±0.01	14	···		31.20±0.10
4382	-1	0.13	1.150±0.022	29.59±0.09	···		···		···		···		···		···		31.07±0.11
4406	-5	0.13	1.167±0.008	29.51±0.12	32.11±0.10	2	31.23±0.06	2	25.45±0.10	7	···		30.10±0.03	14	26.26±0.06	12	31.22±0.07
4472	-5	0.10	1.218±0.011	29.62±0.07	32.26±0.06	2	31.27±0.06	2	25.30±0.11	7	25.25±0.13	8	29.99±0.02	14	26.26±0.04	12	31.07±0.08
4486	-4	0.10	1.244±0.012	29.72±0.14	···		···		···		···		30.07±0.03	14	···		30.97±0.10
4494	-5	0.09	1.139±0.010	29.38±0.08	···		···		···		···		···		···		30.81±0.08
4565	3	0.07	1.128±0.027	29.37±0.11	···		···		···		···		···		25.53±0.08	12	30.63±0.12
4649	-5	0.12	1.232±0.023	29.76±0.09	···		···		···		···		30.21±0.07	14	···		31.09±0.08

Table 8—Continued

Galaxy	T[a]	A_B[a]	$(V-I)_0$[a]	$\bar{m}_I$[a]	$\bar{m}_V$	Ref.	$\bar{m}_R$	Ref.	$\bar{m}_{K'}$	Ref.	$\bar{m}_{Ks}$	Ref.	$\bar{m}_{F814W}$	Ref.	$\bar{m}_{F160W}$	Ref.	DM
N4660	-5	0.14	1.154±0.015	28.82±0.17	···		···		···		···		30.11±0.09	14	···		30.70±0.08
N5102	-3	0.24	0.976±0.016	25.49±0.09	···		···		···		···		···		···		27.89±0.13
N5128	-2	0.50	1.078±0.016	26.05±0.11	28.12±0.06	4	···		···		···		···		···		27.90±0.08
N5195	0	0.16	1.056±0.019	27.25±0.25	···		···		···		···		···		···		29.37±0.08

Note. — References: (1)=Ajhar & Tonry 1994; (2)=Tonry, Ajhar & Luppino 1990; (3)=Blakeslee, Vazdekis & Ajhar 2001; (4)=Tonry & Schetcher 1990; (5)=Jensen et 1996; (6)=Luppino & Tonry 1993; (7)=Jensen et al. 1998; (8)=Pahre & Mould 1994; (9)=Mei et al. 2001; (10)=Liu, Graham & Charlot 2001; (11)=Ajhar et al. 1997; 2)=Jensen et al. 2003; (13)=Pahre et al. 1999; (14)=Neilsen & Tsvetanov 2000

[a]Data from T01

[b]Freedman et al. 2001, Table 3

Table 9. Age and metallicity extimations of selected galaxies

Galaxy (1)	DM (2)	Age[a] (3)	[Fe/H][a] (4)	Age[b] (5)	[Fe/H][b] (6)	Age^{SBF}_{mag} (7)	$[\mathrm{Fe/H}]^{SBF}_{mag}$ (8)	$\mathrm{Age}^{SBF}_{color}$ (9)	$[\mathrm{Fe/H}]^{SBF}_{color}$ (10)
NGC 0221	24.44 ± 0.10	3.8	-0.04	4.9±1.3	-0.01±0.05	5-9	$\sim$0.00	6	0.04
NGC 0224	24.44 ± 0.07	5.1	0.42	···	···	$\sim$15	$\sim$0.00	12	0.15
NGC 0891	29.96 ± 0.06	11	-0.47	···	···	11-13	~ -0.27	···	···
NGC 1316	31.49 ± 0.03	3.4	0.25	···	···	$\sim$5	$\sim$0.00	···	···
NGC 1399	31.49 ± 0.03	···	>0.5	···	···	$\gtrsim 10$	$\gtrsim 0.00$	12	0.12
NGC 1404	31.49 ± 0.03	5.9	0.47	···	···	5-9	$\gtrsim 0.00$	9	0.20
NGC 3115	30.14 ± 0.16	···	>0.5	···	···	$\sim$13	$0.00/-0.27$	···	···
NGC 3377	30.09 ± 0.04	4.1	0.20	5.9±1.2	-0.28±0.04	$\sim$5	0.00	···	···
NGC 3379	30.09 ± 0.04	9.3	0.16	13.2±2.4	-0.17±0.04	9-13	$\sim$0.00	12	0.00
NGC 3384	30.09 ± 0.04	···	>0.5	···	···	$\sim$5	0.00/0.33[c]	···	···
						13	-0.27[d]		
NGC 4278	31.11 ± 0.09	10.7	0.14	···	···	5-9	0.00[c]	···	···
						13-15	-0.27[d]		
NGC 4374	30.97 ± 0.04	11.8	0.12	14.4±2.8	-0.19±0.05	5-11	$\gtrsim 0.00$	8	0.15
NGC 4382	30.97 ± 0.04	1.6	0.44	···	···	$\lesssim 5$	$\gtrsim 0.33$	···	···
NGC 4472	31.01 ± 0.04	8.5	0.24	8.4±2.7	0.00±0.06	$\gtrsim 7$	$\gtrsim 0.00$	9	0.20
NGC 4649	31.54 ± 0.08	11	0.30	18.3±2.8	-0.22 ± 0.04	···	···	···	···

[a]Terlevich & Forbes 2002, Table 2

[b]Trager et al. 2000, Table 6B: model 4

[c]Estimations from $\bar{M}_I$

[d]Estimations from $\bar{M}_{F160W}$

Table A1. SBF predictions for a stellar population with $t = 15\ Gyr$ and $Z = Z_{\odot}$ as function of the total number of stars N_{star}. The last row indicates the SBF amplitudes as computed by using the "usual" approach.

N_{star}	V_{tot}	$\bar{M}_B$	$\bar{M}_V$	$\bar{M}_I$	$\bar{M}_K$	$(V-I)_0$
10^3	0.455	2.236	0.710	-1.551	-5.373	1.055
10^4	-2.292	2.365	0.795	-1.504	-5.408	1.192
10^5	-4.822	2.353	0.781	-1.513	-5.402	1.233
10^6	-7.325	2.407	0.839	-1.473	-5.403	1.235
$5 \cdot 10^6$	-9.074	2.395	0.831	-1.483	-5.410	1.235
$2.6 \cdot 10^7$	-10.847	2.469	0.910	-1.474	-5.414	1.235
$2.1 \cdot 10^8$	-13.098	2.589	0.989	-1.391	-5.365	1.235
"usual"	$\cdots$	2.599	1.040	-1.371	-5.381	$\cdots$

This figure "Cantiello.fig1.jpg" is available in "jpg" format from:

http://arXiv.org/ps/astro-ph/0303325v1

This figure "Cantiello.fig2.jpg" is available in "jpg" format from:

http://arXiv.org/ps/astro-ph/0303325v1

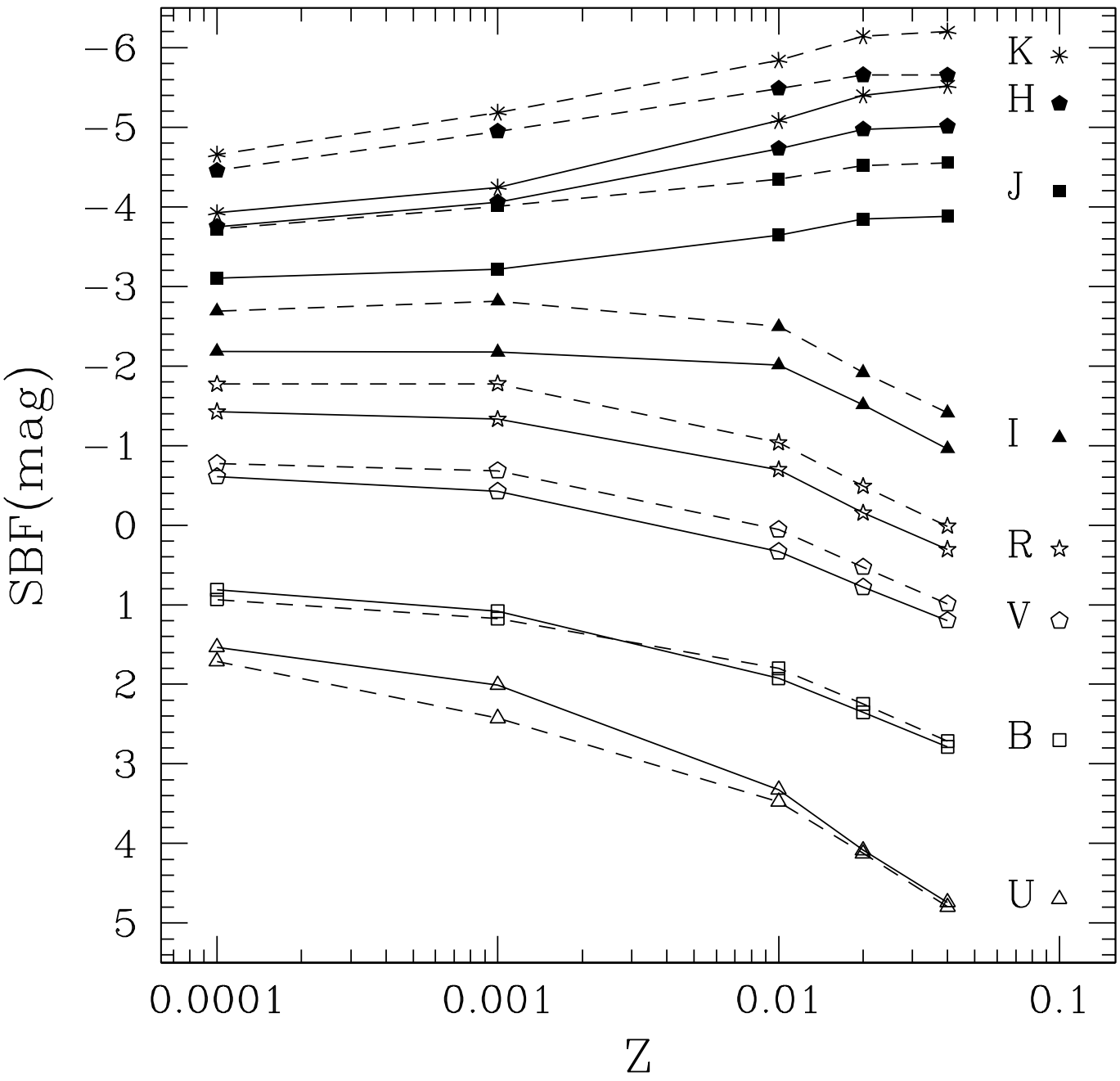
SBF(mag)
−6
−5
−4
−3
−2
−1
0
1
2
3
4
5
0.0001
0.001
0.01
0.1
Z
K
H
J
I
R
V
B
U

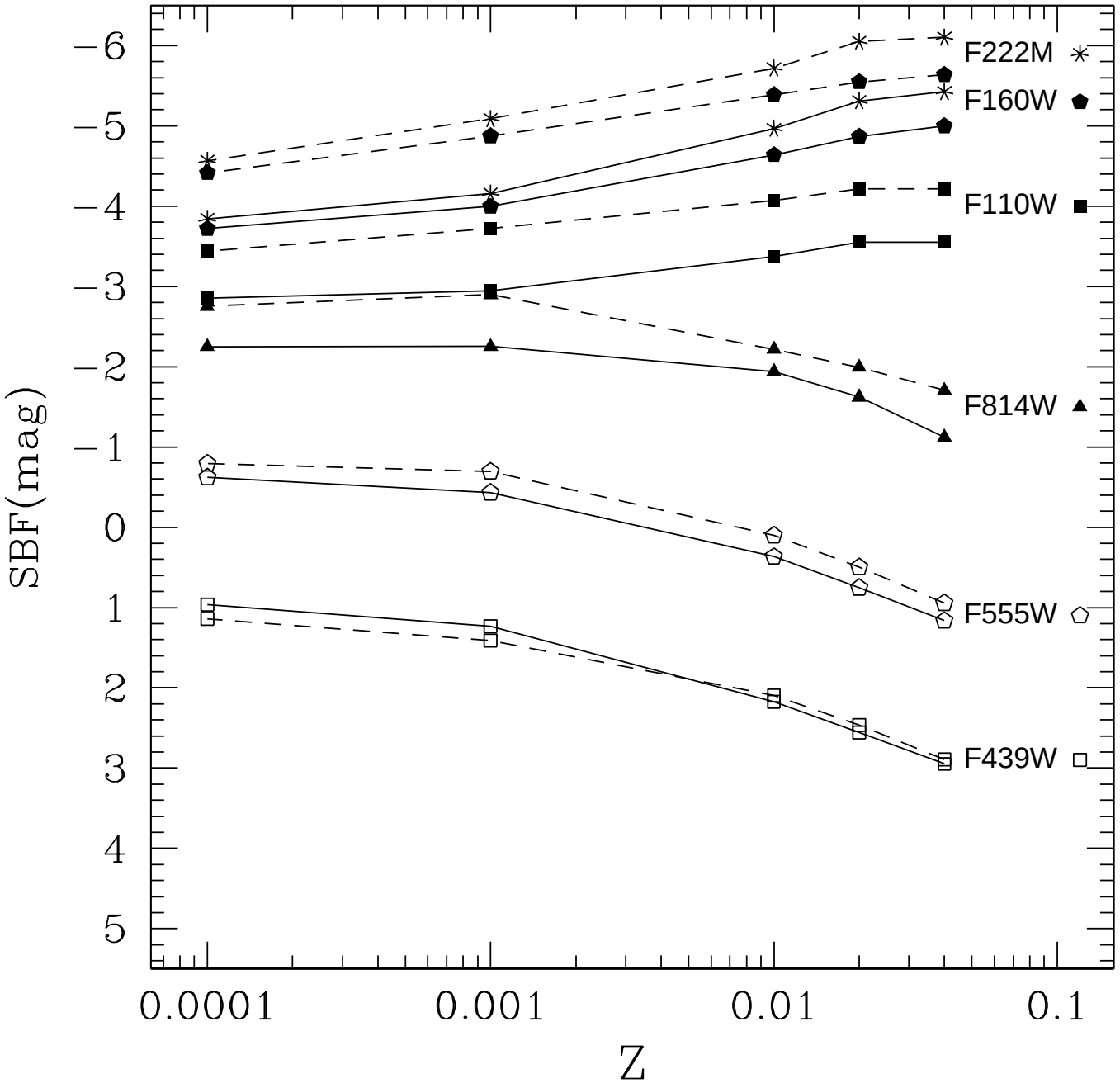
F222M
F160W
F110W
F814W
F555W
F439W
SBF(mag)
−6
−5
−4
−3
−2
−1
0
1
2
3
4
5
0.0001
0.001
0.01
0.1
Z

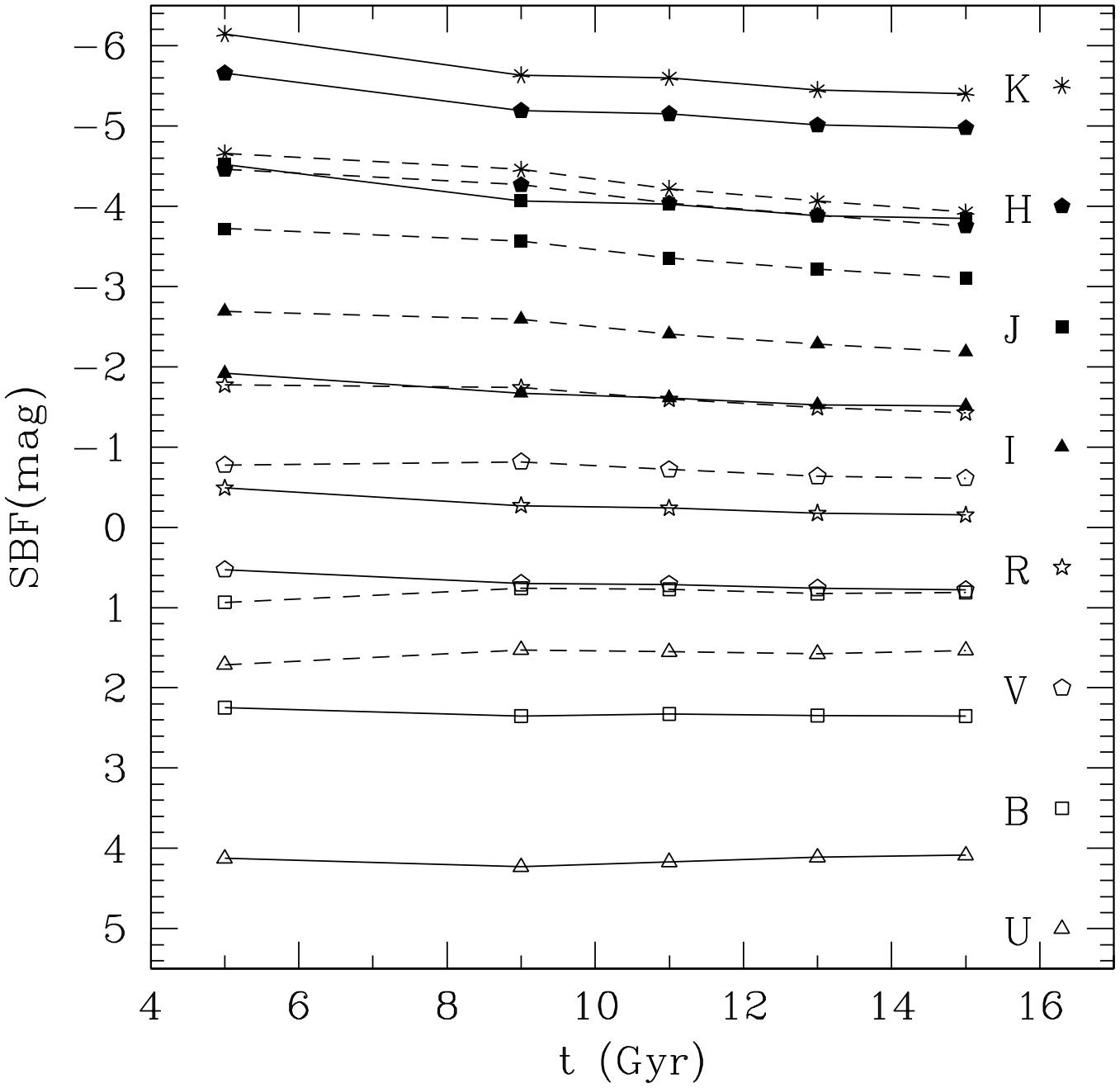
SBF(mag)
−6
−5
−4
−3
−2
−1
0
1
2
3
4
5
4
6
8
10
12
14
16
t (Gyr)
K
H
J
I
R
V
B
U

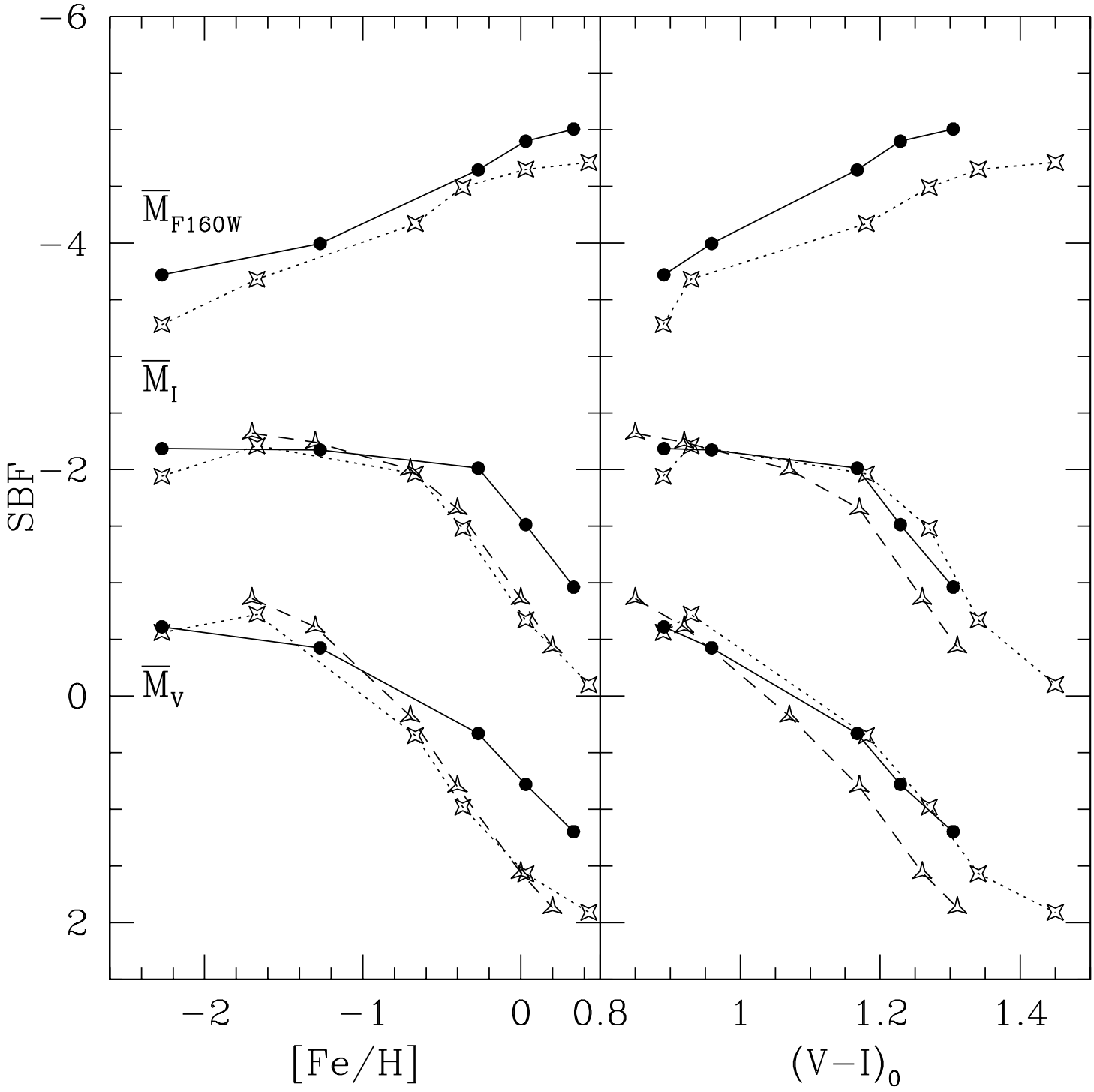
−6
−4
−2
0
2
SBF
$\overline{M}_{F160W}$
$\overline{M}_I$
$\overline{M}_V$
−2
−1
0
0.8
1
1.2
1.4
[Fe/H]
$(V-I)_0$

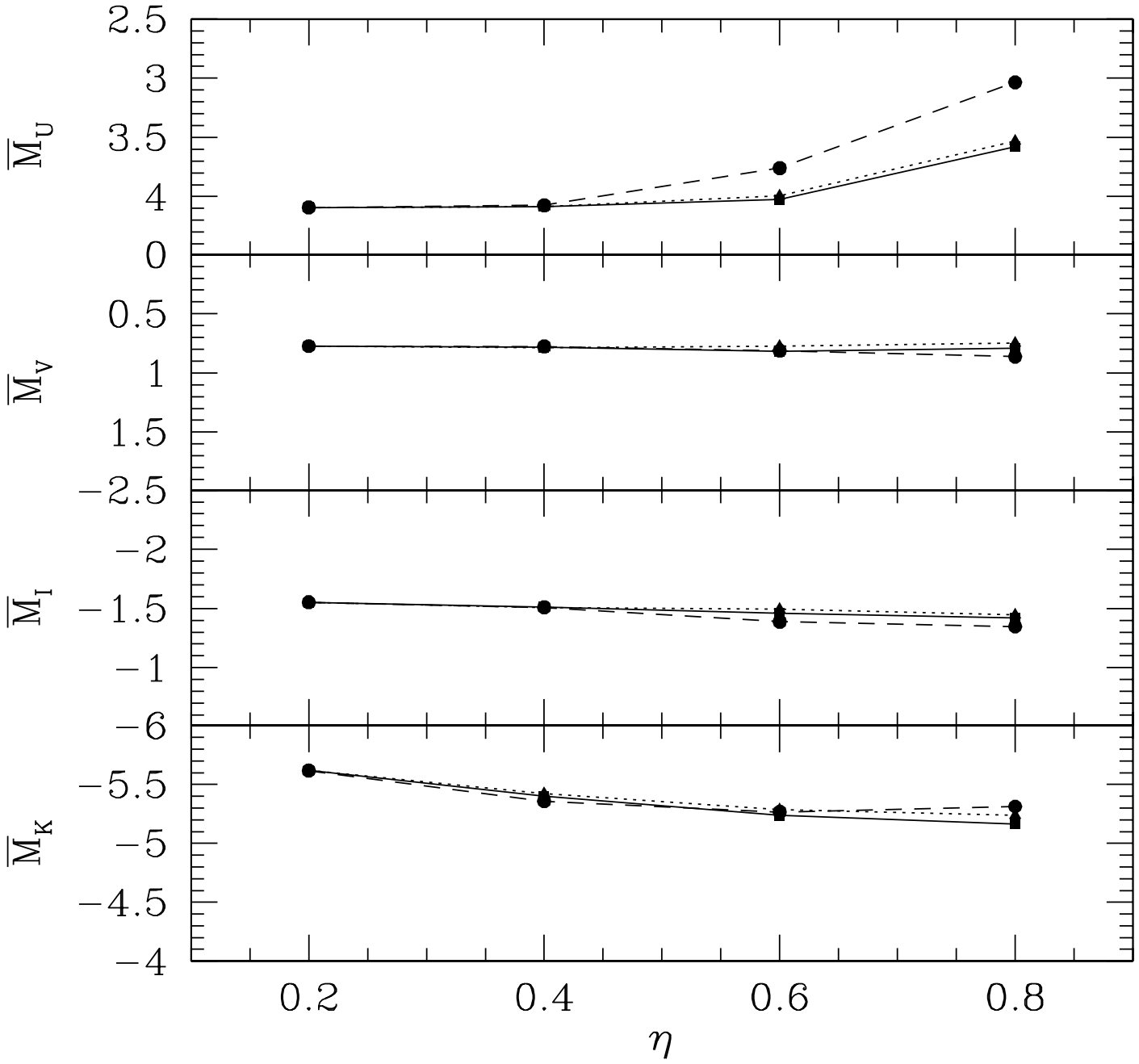
2.5
3
3.5
4
$\overline{M}_U$
0
0.5
1
1.5
$\overline{M}_V$
−2.5
−2
−1.5
−1
$\overline{M}_I$
−6
−5.5
−5
−4.5
$\overline{M}_K$
−4
0.2
0.4
0.6
0.8
η

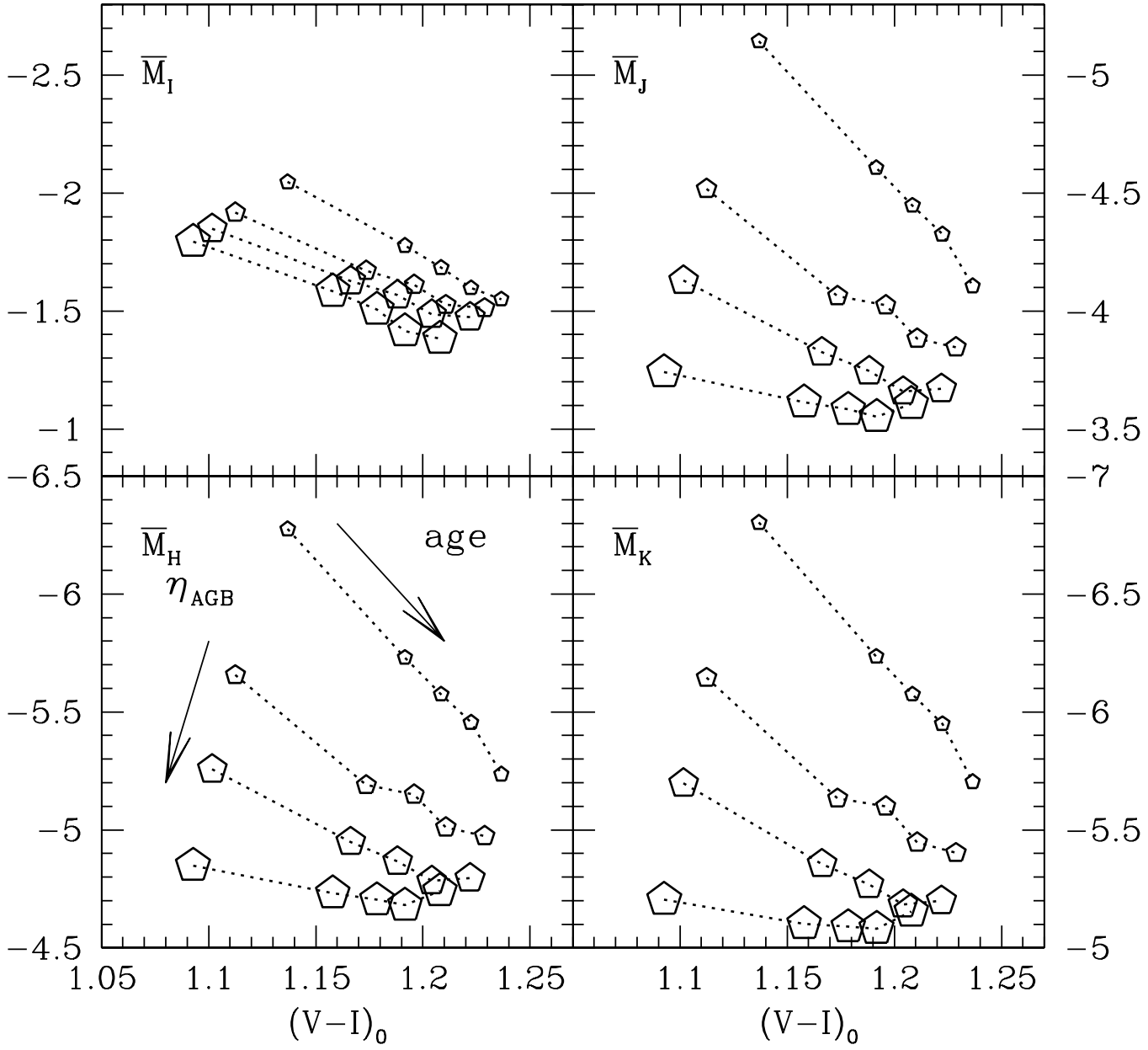
$\overline{M}_I$
$\overline{M}_J$
$\overline{M}_H$
η_{AGB}
age
$\overline{M}_K$
−2.5
−2
−1.5
−1
−6.5
−5
−4.5
−4
−3.5
−7
−6
−5.5
−5
−4.5
−6.5
−6
−5.5
−5
1.05
1.1
1.15
1.2
1.25
$(V-I)_0$

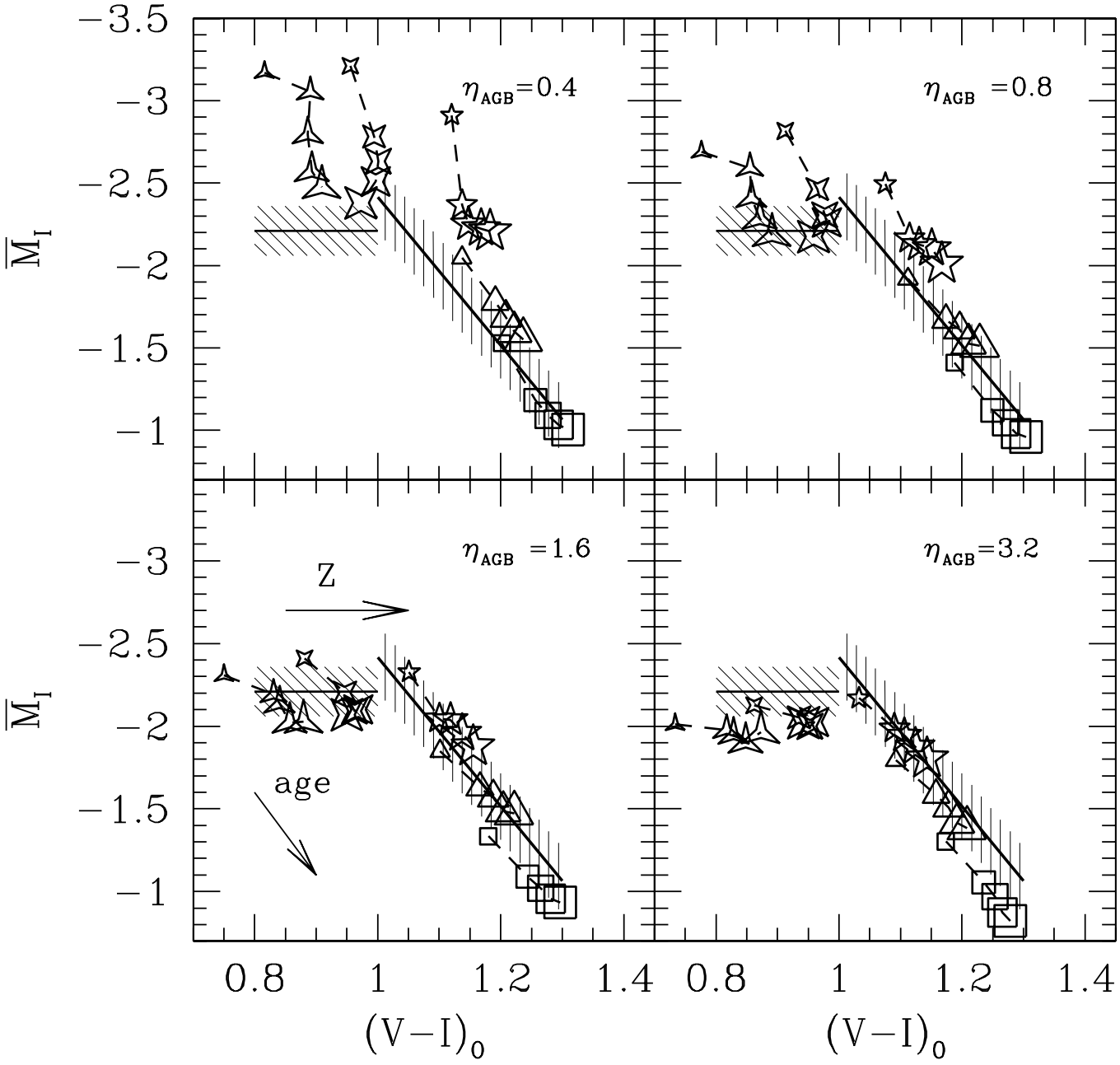
η_{AGB}=0.4
η_{AGB} =0.8
η_{AGB} =1.6
η_{AGB}=3.2
Z
age
$\overline{M}_I$
$(V-I)_0$
−3.5
−3
−2.5
−2
−1.5
−1
0.8
1
1.2
1.4

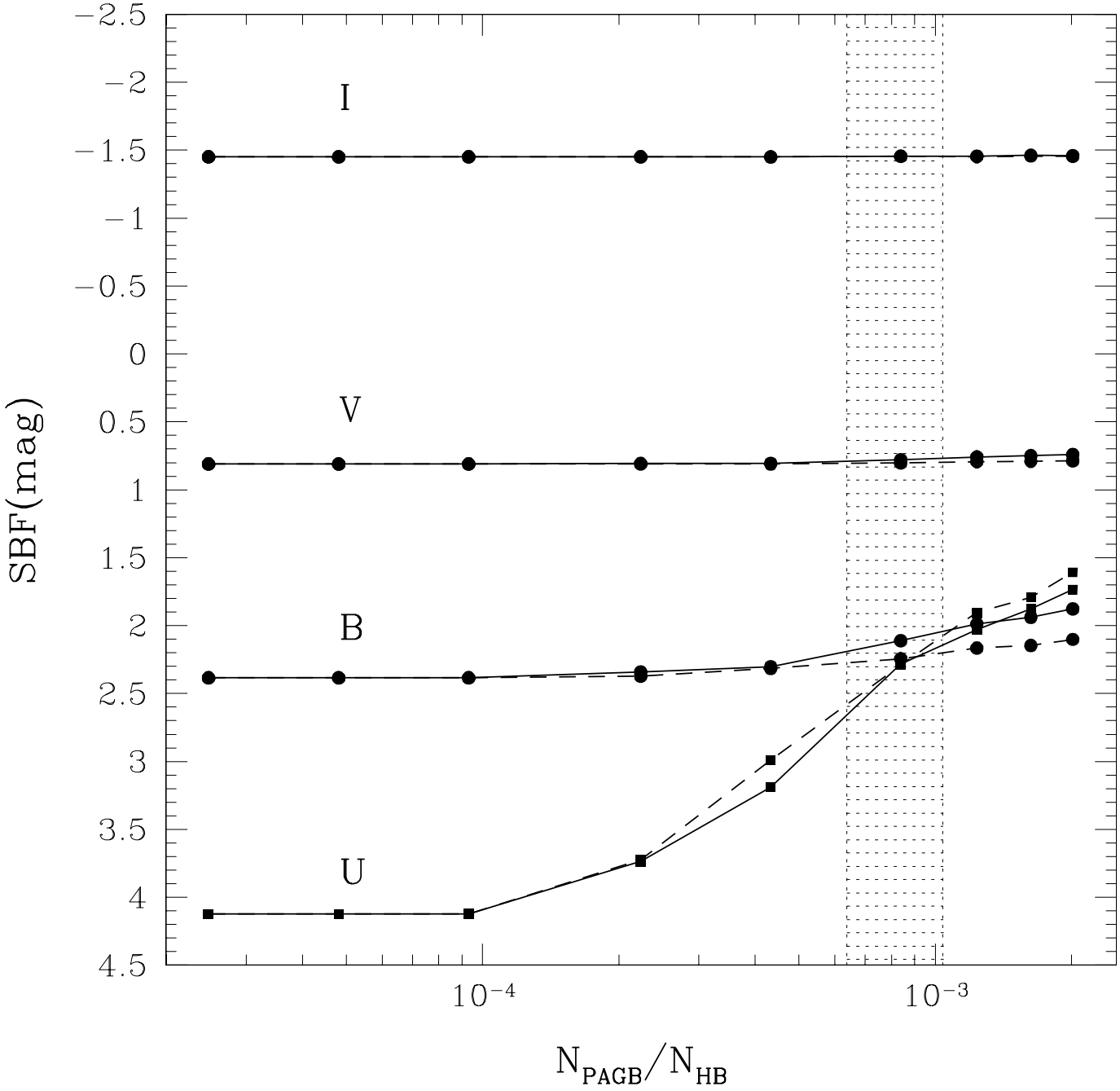
−2.5
−2
−1.5
−1
−0.5
0
0.5
1
1.5
2
2.5
3
3.5
4
4.5
I
V
B
U
SBF(mag)
10^{-4}
10^{-3}
N_{PAGB}/N_{HB}

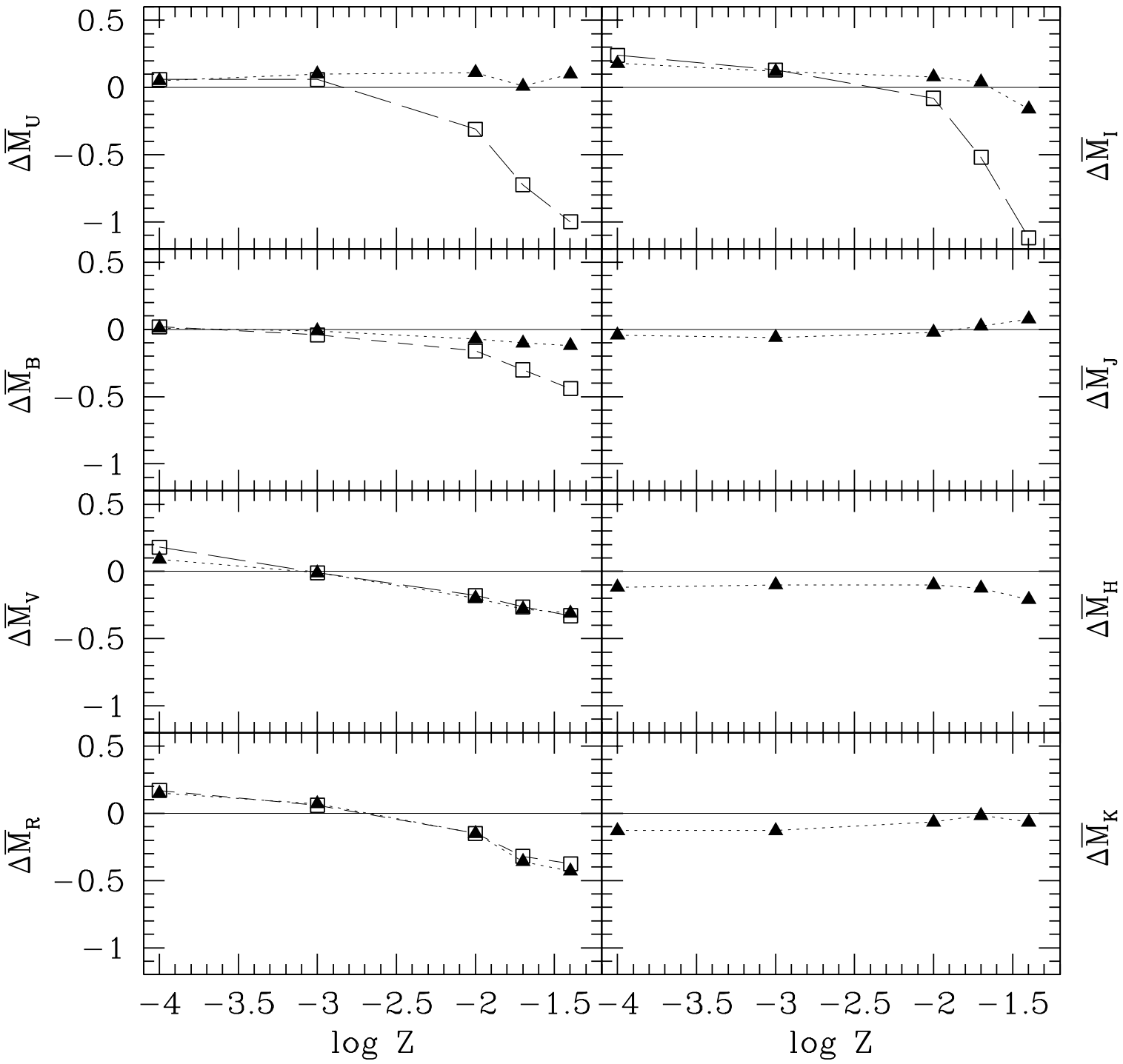
0.5
0
−0.5
−1
$\Delta\overline{M}_U$
$\Delta\overline{M}_I$
$\Delta\overline{M}_B$
$\Delta\overline{M}_J$
$\Delta\overline{M}_V$
$\Delta\overline{M}_H$
$\Delta\overline{M}_R$
$\Delta\overline{M}_K$
−4 −3.5 −3 −2.5 −2 −1.5
log Z

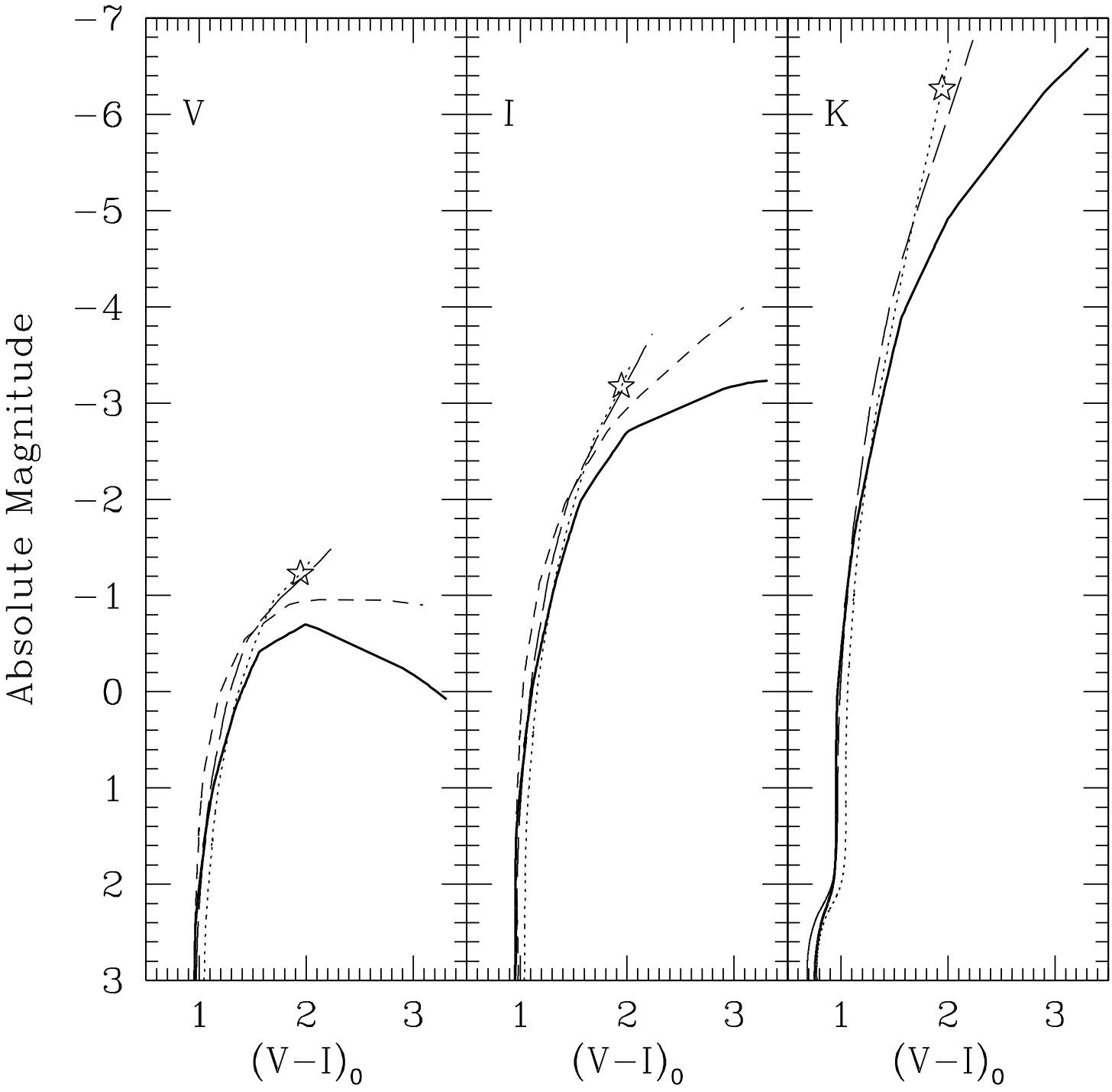
V
I
K
Absolute Magnitude
−7
−6
−5
−4
−3
−2
−1
0
1
2
3
1
2
3
(V−I)0

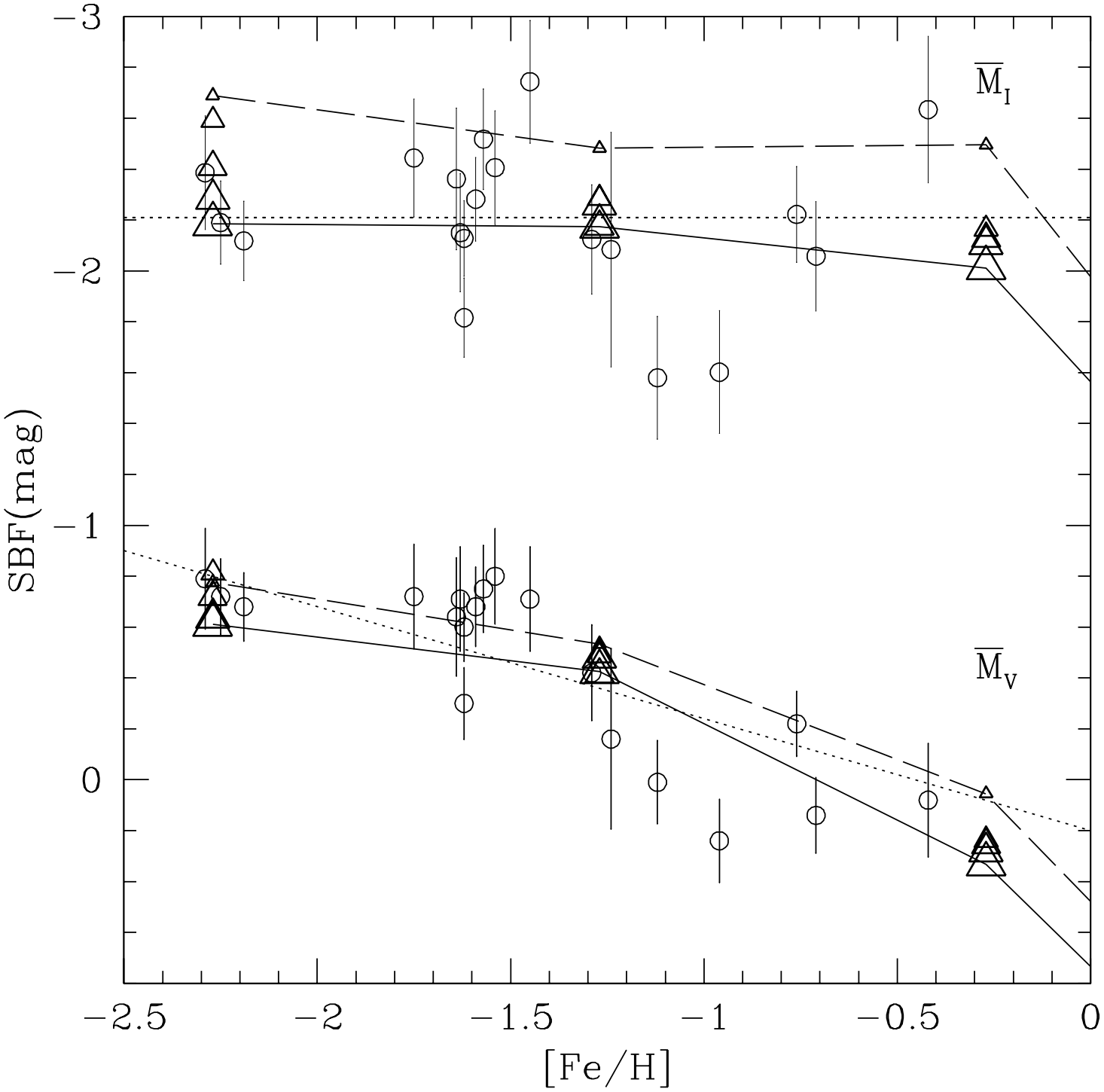
−3
−2
−1
0
SBF(mag)
$\overline{M}_I$
$\overline{M}_V$
−2.5
−2
−1.5
−1
−0.5
0
[Fe/H]

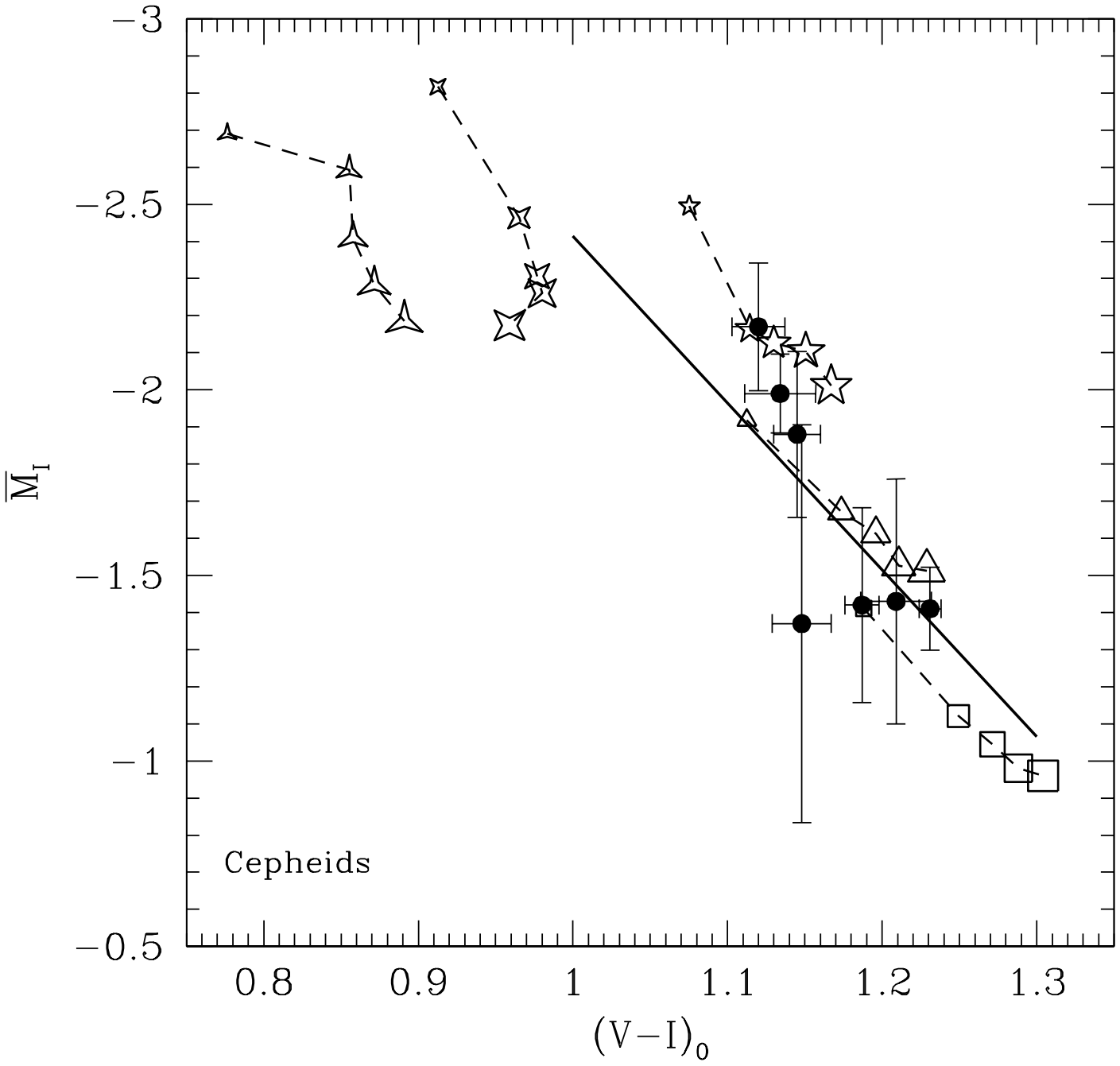
−3
−2.5
−2
−1.5
−1
−0.5
$\overline{M}_I$
0.8
0.9
1
1.1
1.2
1.3
$(V-I)_0$
Cepheids

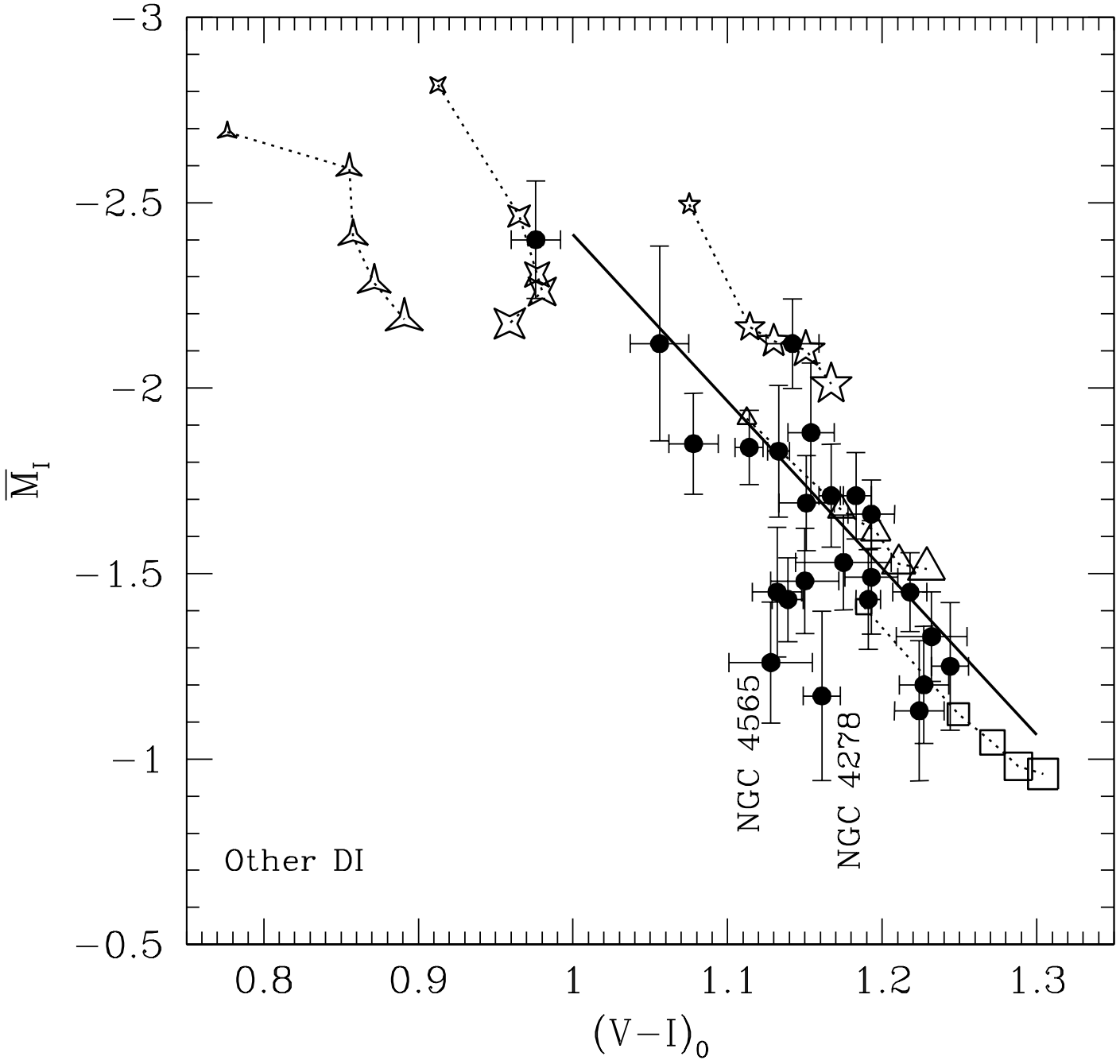
−3
−2.5
−2
−1.5
−1
−0.5
0.8
0.9
1
1.1
1.2
1.3
$\overline{M}_I$
$(V-I)_0$
NGC 4565
NGC 4278
Other DI

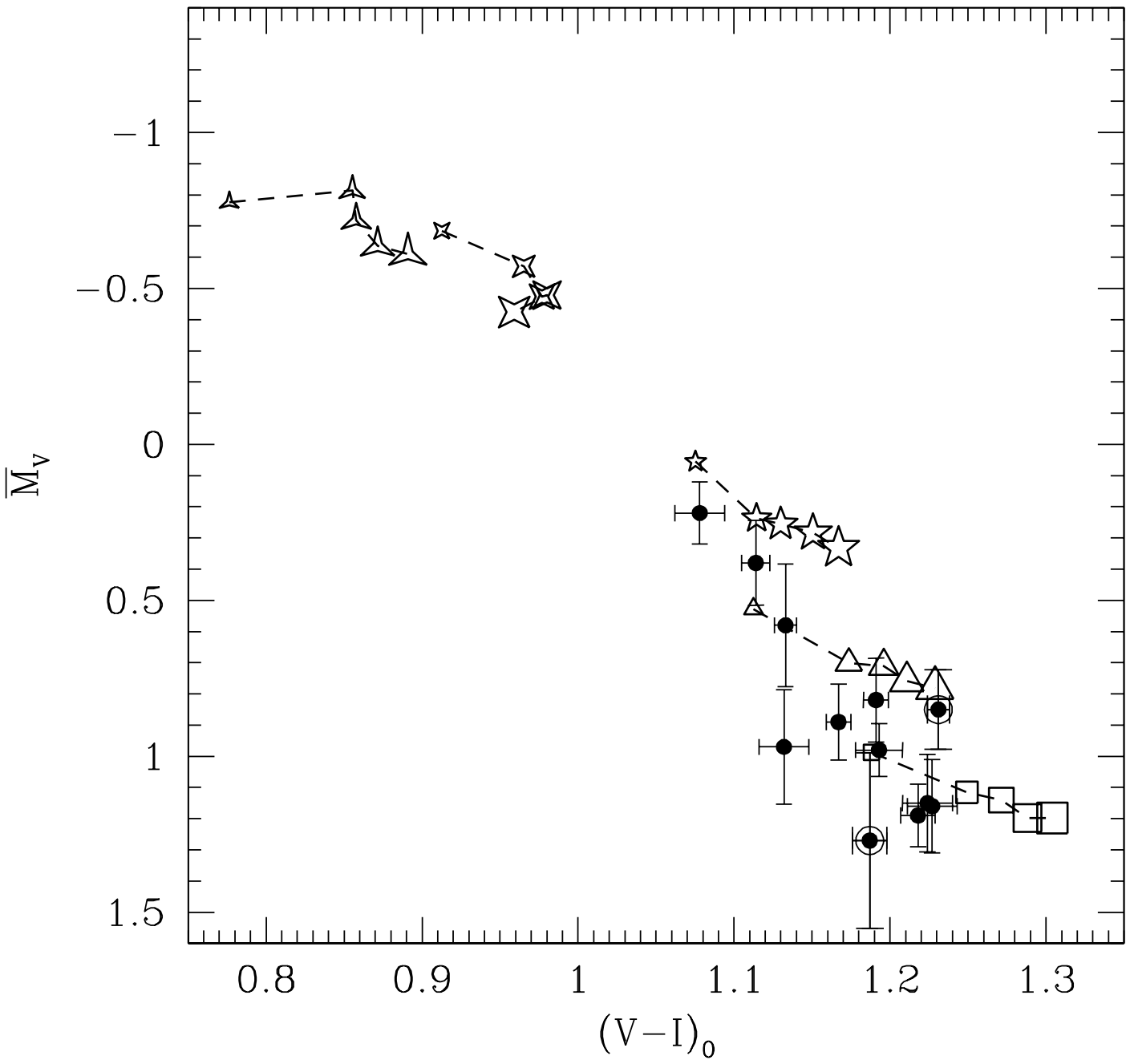
−1
−0.5
0
0.5
1
1.5
$\overline{M}_V$
0.8
0.9
1
1.1
1.2
1.3
$(V-I)_0$

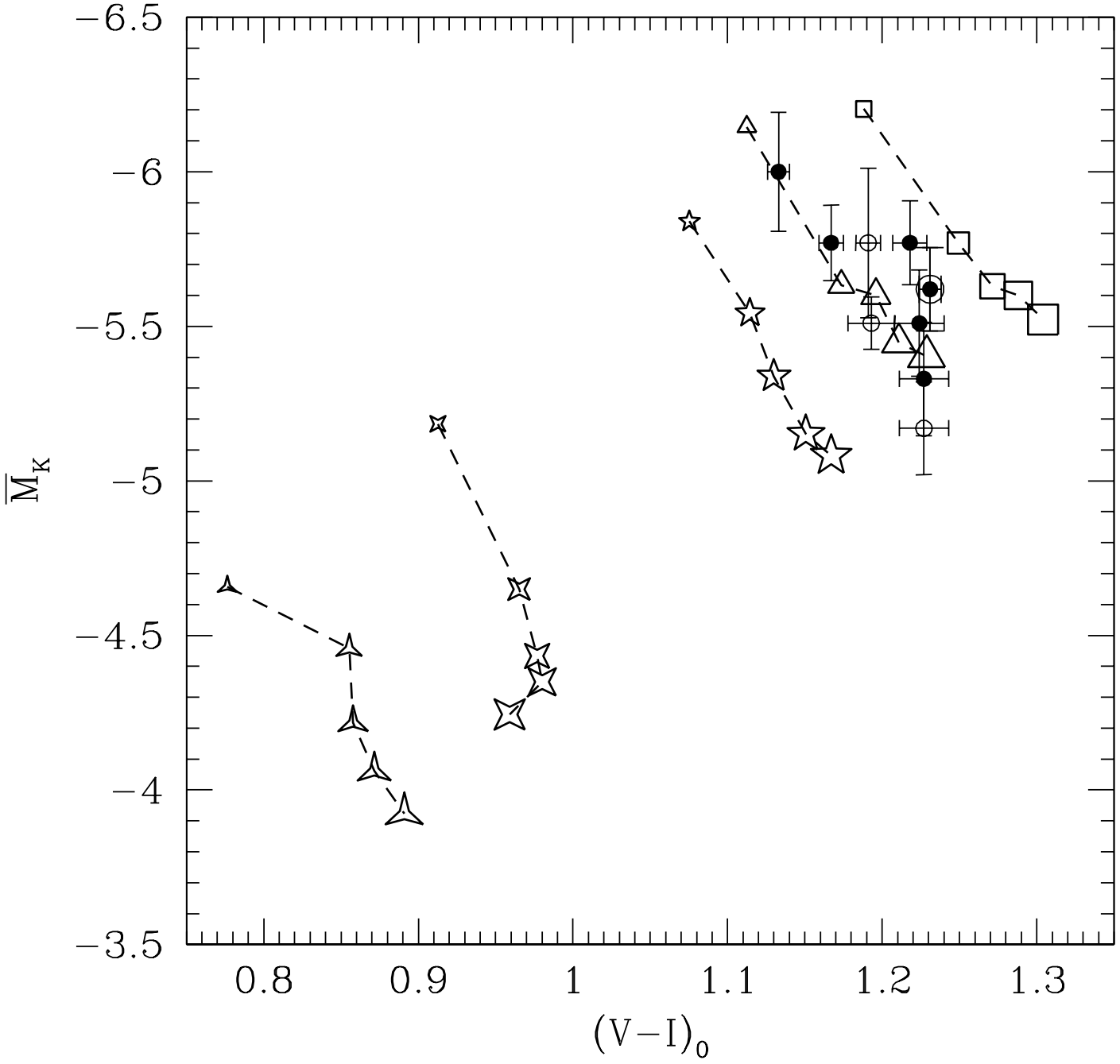
−6.5
−6
−5.5
−5
−4.5
−4
−3.5
$\overline{M}_K$
0.8
0.9
1
1.1
1.2
1.3
$(V-I)_0$

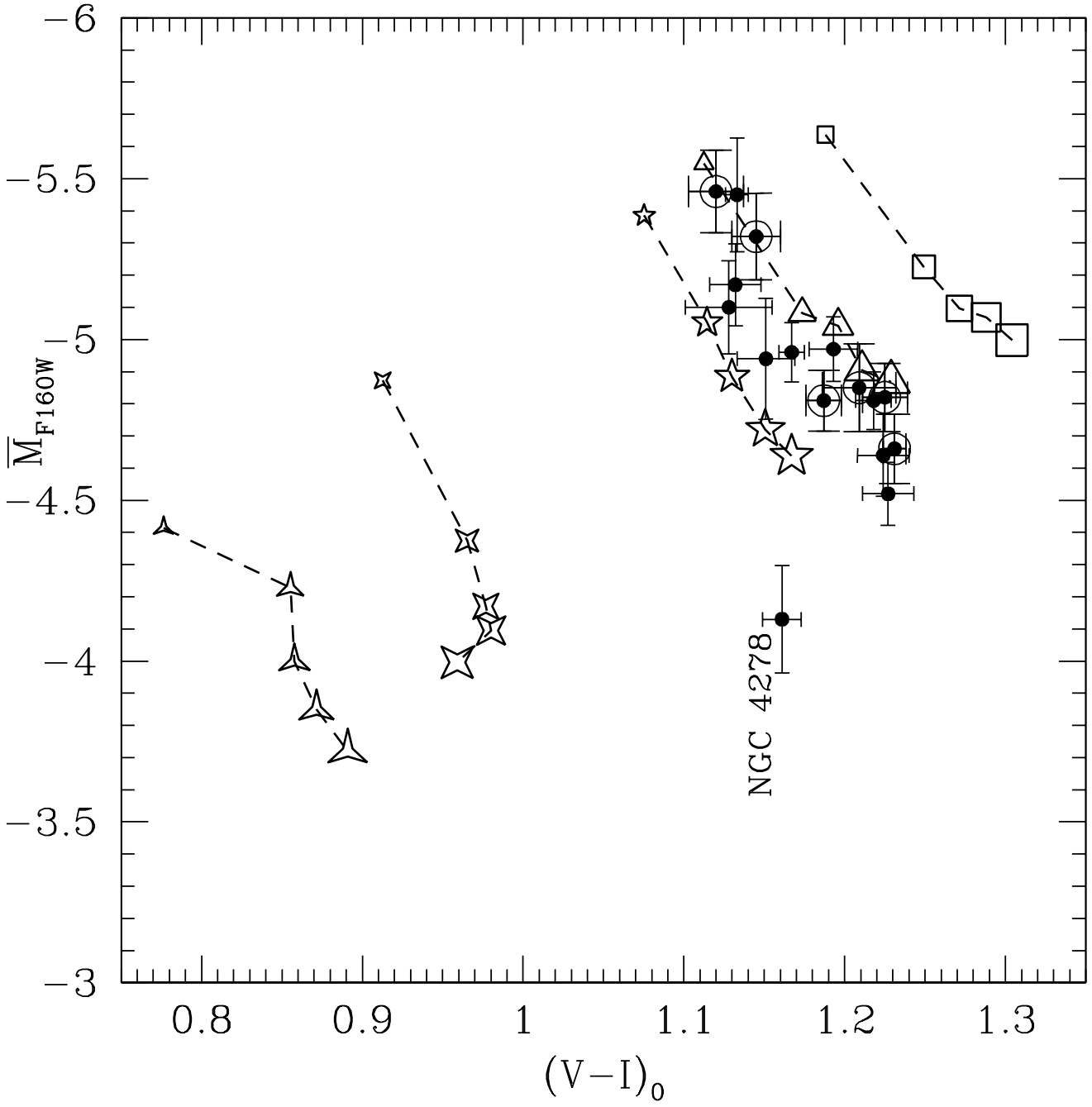
−6
−5.5
−5
−4.5
−4
−3.5
−3
0.8
0.9
1
1.1
1.2
1.3
$\overline{M}_{F160W}$
$(V-I)_0$
NGC 4278

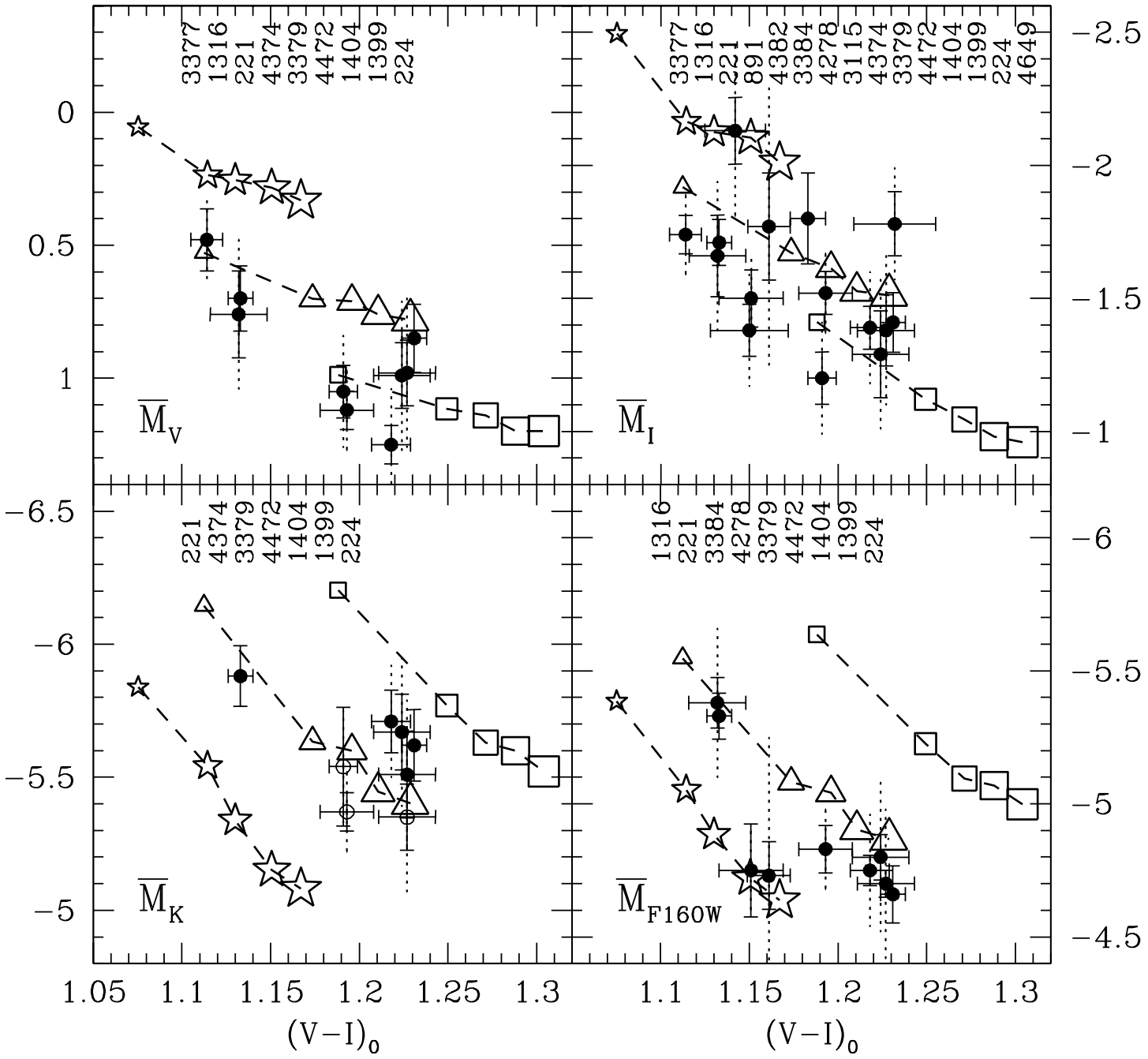
3377
1316
221
4374
3379
4472
1404
1399
224
$\overline{M}_V$
0
0.5
1
3377
1316
221
891
4382
3384
4278
3115
4374
3379
4472
1404
1399
224
4649
$\overline{M}_I$
−2.5
−2
−1.5
−1
221
4374
3379
4472
1404
1399
224
$\overline{M}_K$
−6.5
−6
−5.5
−5
1316
221
3384
4278
3379
4472
1404
1399
224
$\overline{M}_{F160W}$
−6
−5.5
−5
−4.5
1.05
1.1
1.15
1.2
1.25
1.3
$(V-I)_0$
1.1
1.15
1.2
1.25
1.3
$(V-I)_0$

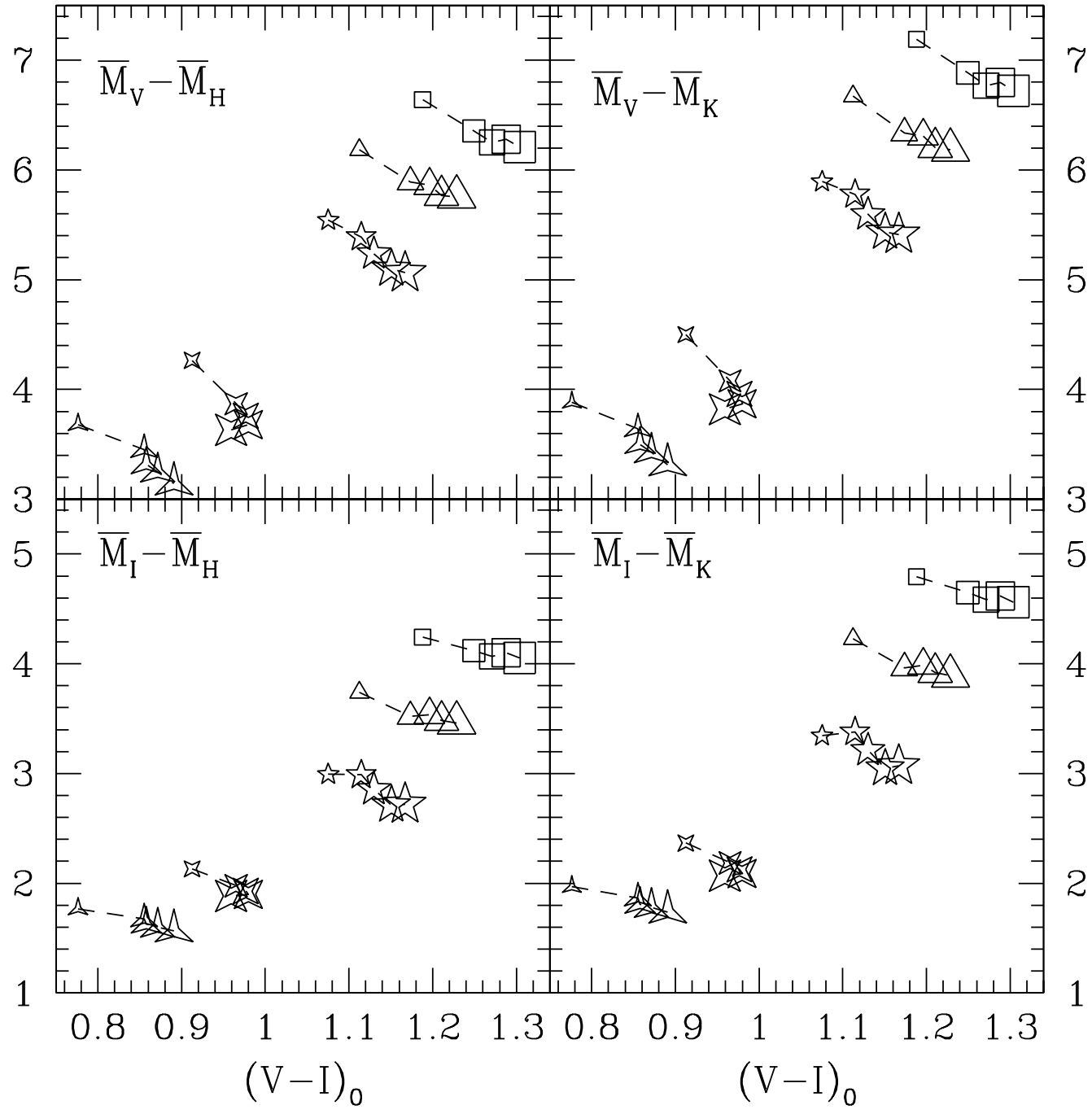
$\overline{M}_V - \overline{M}_H$
$\overline{M}_V - \overline{M}_K$
$\overline{M}_I - \overline{M}_H$
$\overline{M}_I - \overline{M}_K$
7
6
5
4
3
2
1
0.8
0.9
1
1.1
1.2
1.3
$(V-I)_0$

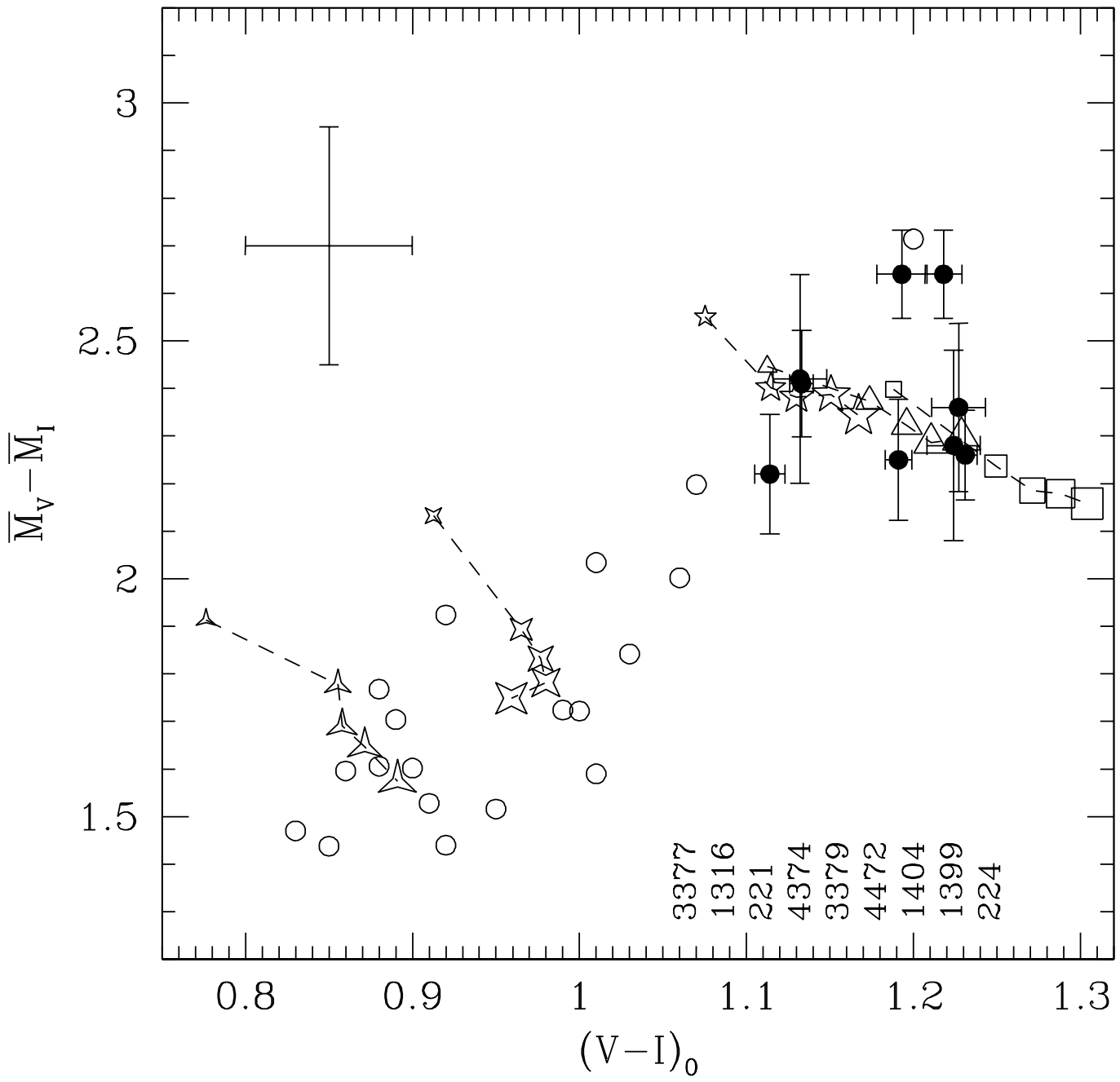
3
2.5
2
1.5
$\overline{M}_V - \overline{M}_I$
0.8
0.9
1
1.1
1.2
1.3
$(V-I)_0$
3377
1316
221
4374
3379
4472
1404
1399
224

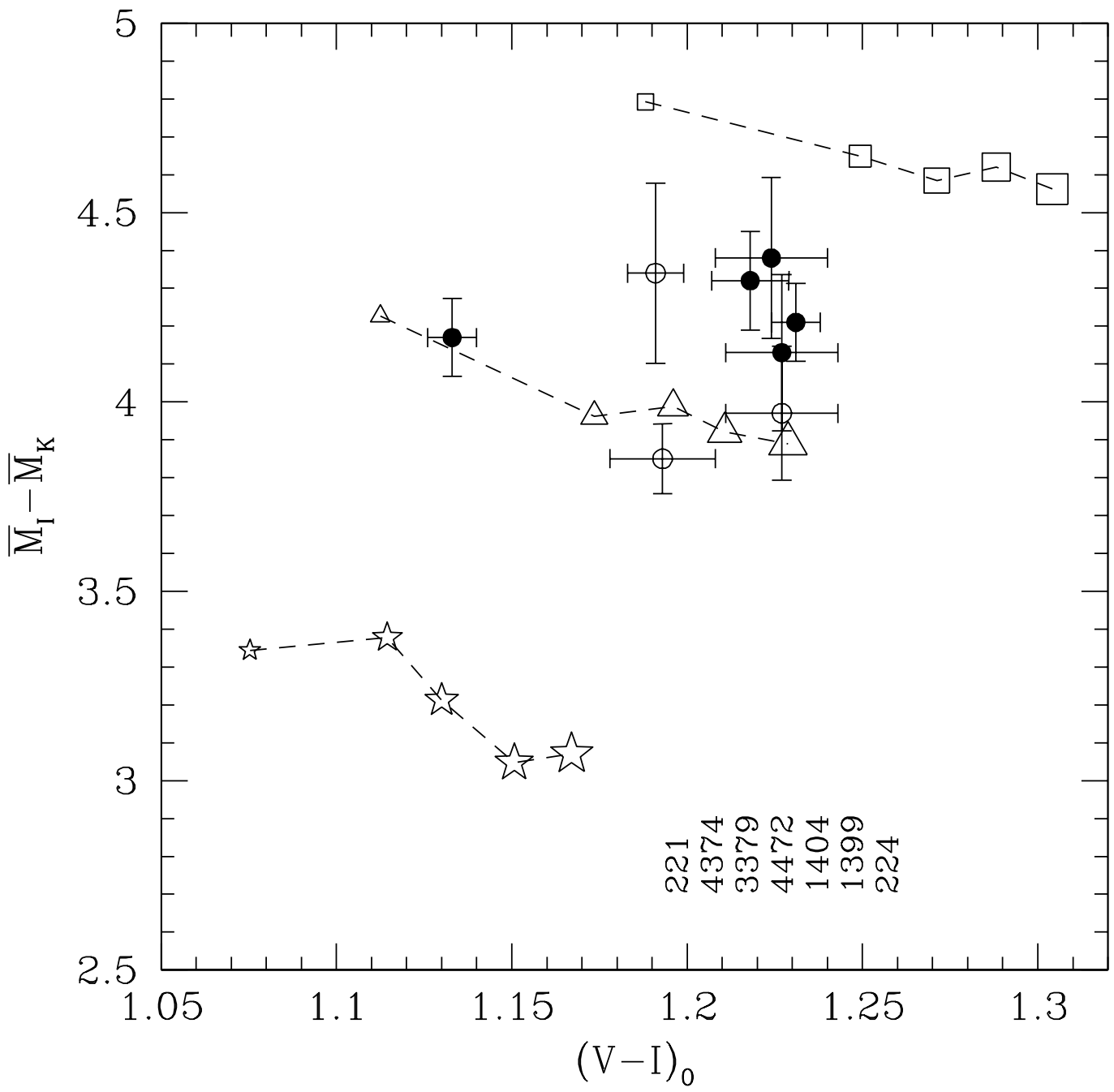
5
4.5
4
3.5
3
2.5
1.05
1.1
1.15
1.2
1.25
1.3
$\overline{M}_I - \overline{M}_K$
$(V-I)_0$
221
4374
3379
4472
1404
1399
224

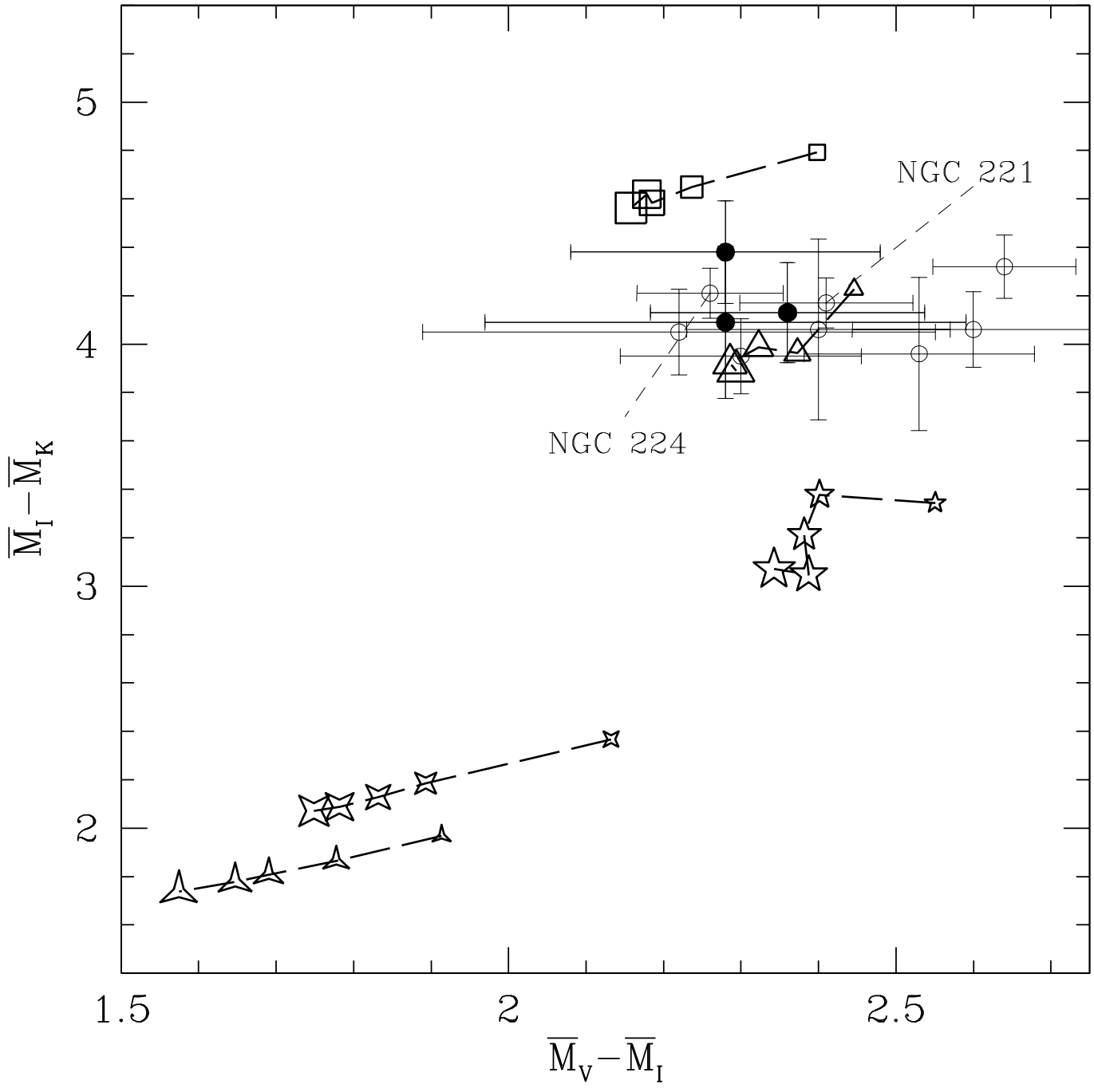
NGC 221
NGC 224
5
4
3
2
1.5
2
2.5
$\overline{M}_I - \overline{M}_K$
$\overline{M}_V - \overline{M}_I$

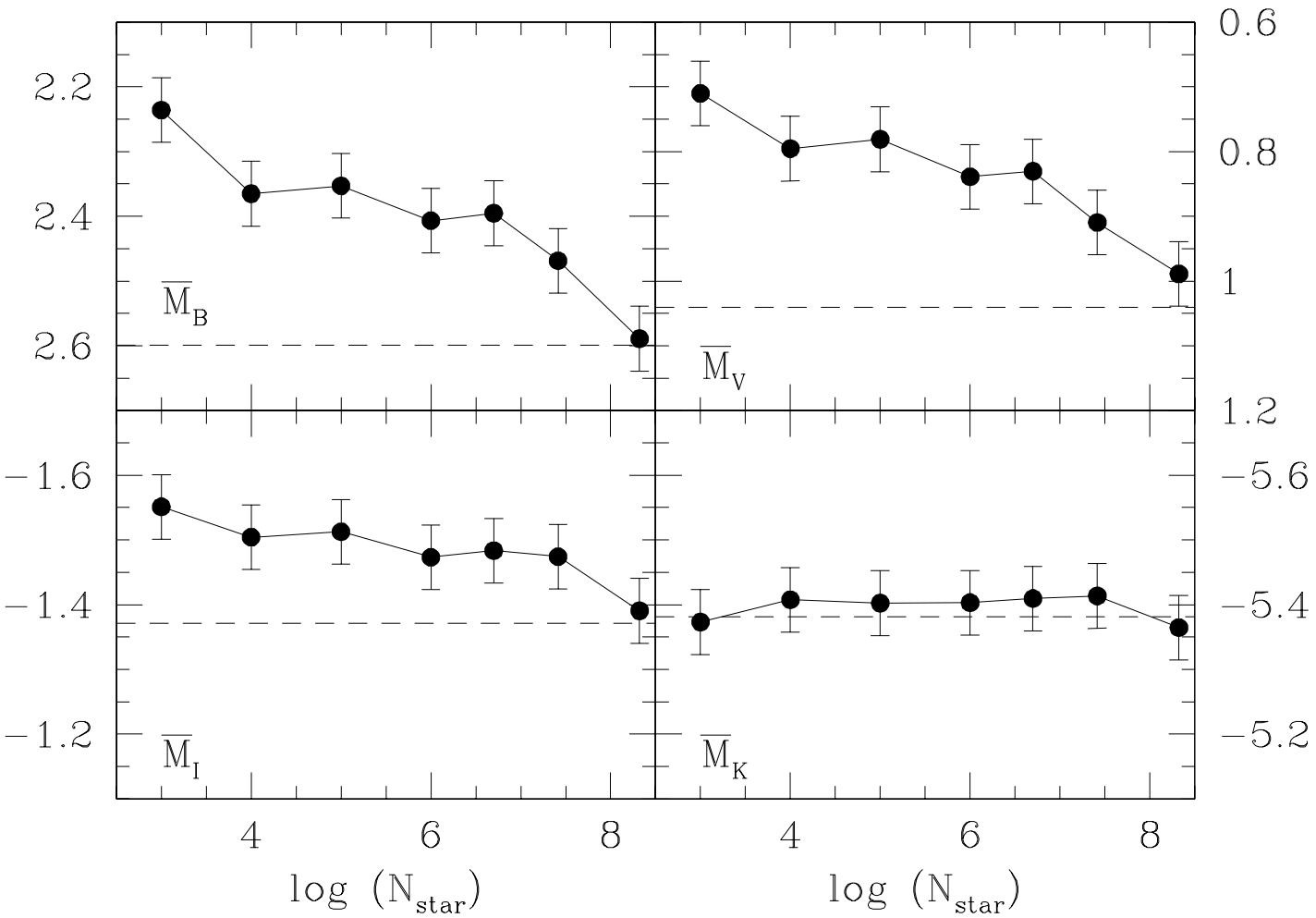
2.2
2.4
2.6
$\overline{M}_B$
0.6
0.8
1
1.2
$\overline{M}_V$
−1.6
−1.4
−1.2
$\overline{M}_I$
−5.6
−5.4
−5.2
$\overline{M}_K$
4
6
8
log (N_{star})
4
6
8
log (N_{star})